

Digital Image Processing and Pattern Recognition Techniques for the Analysis of Fundus Images of the Retina

Rangaraj M. Rangayyan

Department of Electrical and Computer Engineering
University of Calgary
Calgary, Alberta, Canada



SCHULICH
School of Engineering



DEPARTMENT OF ELECTRICAL
AND COMPUTER ENGINEERING

Detection of Blood Vessels in Fundus Images of the Retina

Faraz Oloumi, Rangaraj M. Rangayyan,
Foad Oloumi, Peyman Eshghzadeh-Zanjani, and Fábio J. Ayres

Department of Electrical and Computer Engineering, University of Calgary
Calgary, Alberta, Canada



SCHULICH
School of Engineering



DEPARTMENT OF ELECTRICAL
AND COMPUTER ENGINEERING



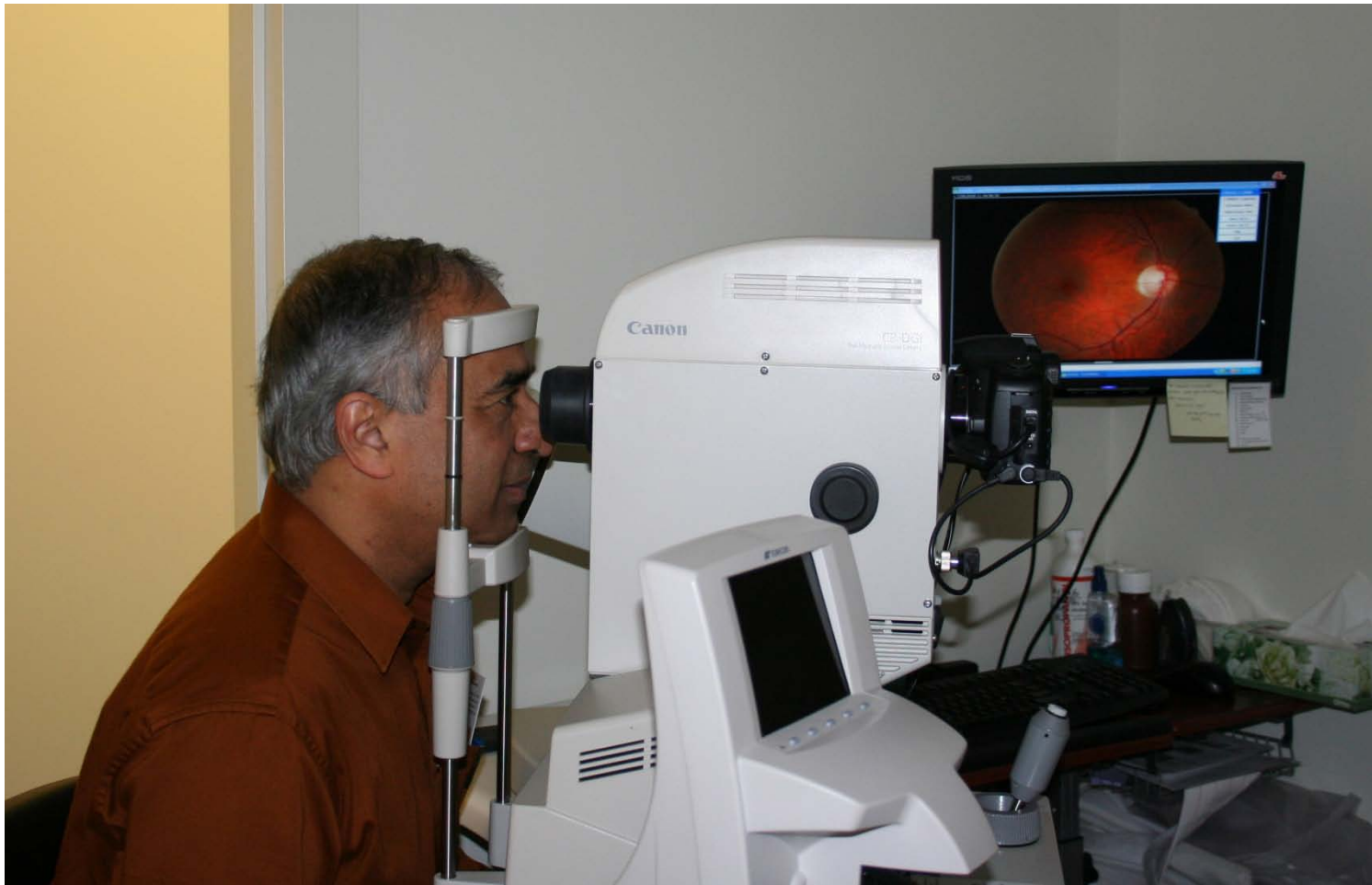
The Retina

- ❖ In embryonic stages of development, the retina and the optic nerve head (ONH) develop as part of the outgrowth of the developing brain.
- ❖ Hence, the retina and the ONH are parts of the central nervous system (CNS).
- ❖ The retina is the only part of the CNS that can be imaged directly and noninvasively.



UNIVERSITY OF
CALGARY

Imaging of the Fundus of the Retina





Fundus Images of the Retina

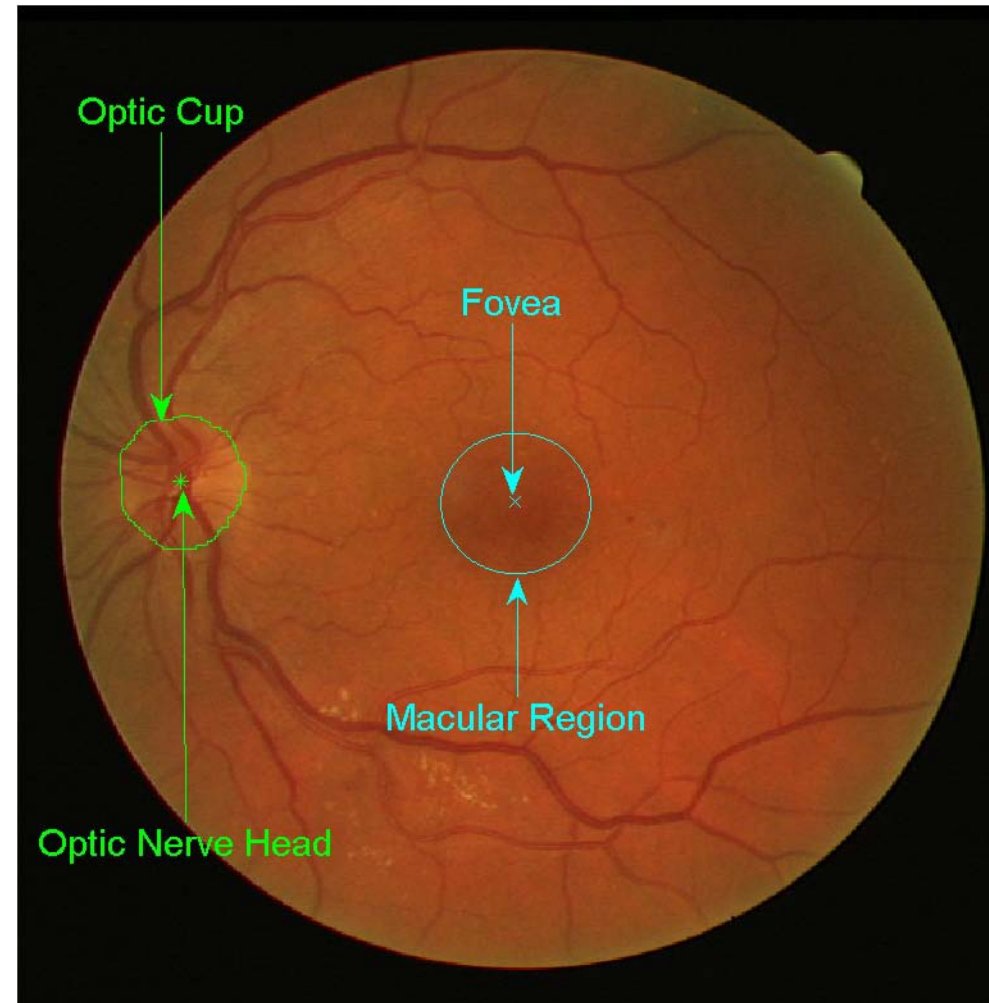
- ❖ The main features of retinal images are the blood vessels.
- ❖ The blood vessels may be used to detect other anatomical features.
- ❖ Statistics of the blood vessels could indicate the presence of diseases.





Fundus Images of the Retina

- ❖ ONH is the point of divergence of blood vessels.
- ❖ The ONH may reflect posterior changes in the retina.
- ❖ Most vessels converge to the macular region, which is usually void of color.





Diseases Affecting the Retina

- ❖ Several diseases and disorders may be detected by analyzing the retina and its features:
 - Diabetic retinopathy,
 - Retinopathy of Prematurity (ROP)
 - Macular degeneration
 - Retinal detachment
 - Hypertension
 - Arteriosclerosis



Abnormal Features in Retinal Images

- ❖ Drusen and white lesions in the macula.
- ❖ Changes in the shape, width, and tortuosity of the blood vessels.
- ❖ Changes in the divergence angle of the vessels at the ONH.
- ❖ Microaneurysms and exudates.



UNIVERSITY OF
CALGARY

Abnormal Features in Retinal Images



Exudates and hemorrhages
STARE im0049



Tortuous vessels
STARE im0198



Analysis of the Retinal Vascular Architecture

Qualitative and quantitative analysis of the architecture of the vasculature could assist in:

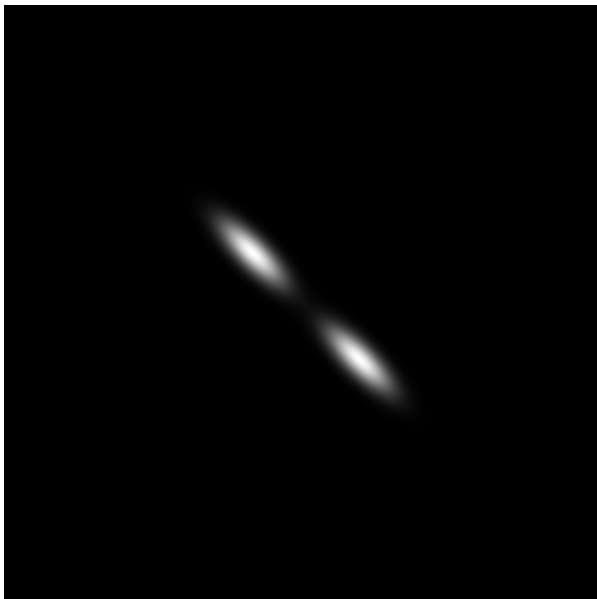
- ❖ Detection of other features and landmarking: ONH and macula.
- ❖ Monitoring the stages of disease processes.
- ❖ Evaluating the effects of treatment.



Detection of Vessels: Gabor Wavelets

Gabor wavelets are sinusoidally modulated Gaussian functions:

provide optimal localization in both the frequency and space domains.



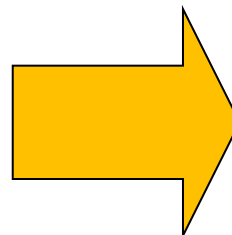


Design of Gabor Filters as Line Detectors

$$g(x, y) = \frac{1}{2\pi\sigma_x\sigma_y} \exp\left[-\frac{1}{2}\left(\frac{x^2}{\sigma_x^2} + \frac{y^2}{\sigma_y^2}\right)\right] \cos(2\pi f x)$$

Design parameters

- line thickness τ
- elongation l
- orientation θ



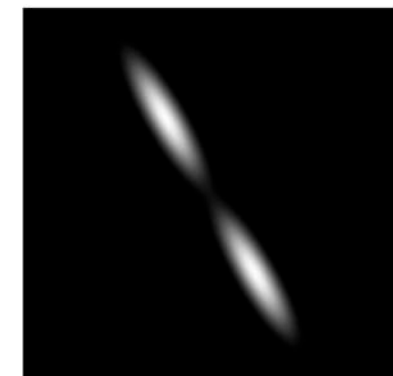
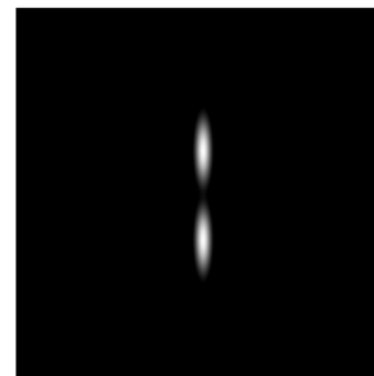
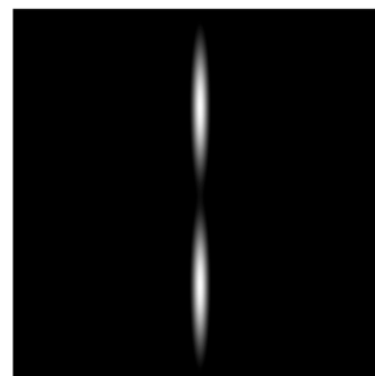
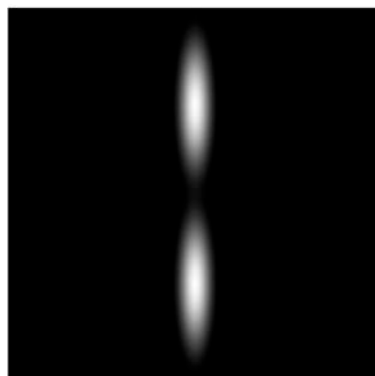
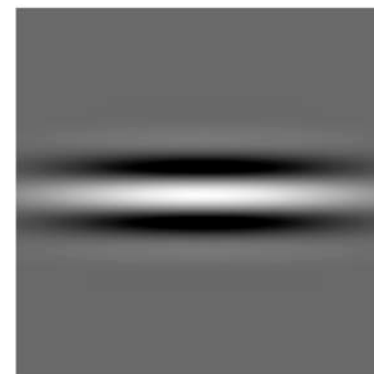
Gabor parameters

$$f = \frac{1}{\tau}; \quad \sigma_x = \frac{\tau}{2\sqrt{2\ln 2}}$$

$$\sigma_y = l\sigma_x; \quad \begin{bmatrix} x \\ y \end{bmatrix} = \begin{bmatrix} \cos \theta & -\sin \theta \\ \sin \theta & \cos \theta \end{bmatrix} \begin{bmatrix} x' \\ y' \end{bmatrix}$$



Gabor Filters: Impulse Response and Frequency Response



$$I = I_0$$

$$\tau = \tau_0$$

$$\theta = \theta_0$$

$$I > I_0$$

$$\tau = \tau_0$$

$$\theta = \theta_0$$

$$I = I_0$$

$$\tau > \tau_0$$

$$\theta = \theta_0$$

$$I = I_0$$

$$\tau = \tau_0$$

$$\theta > \theta_0$$



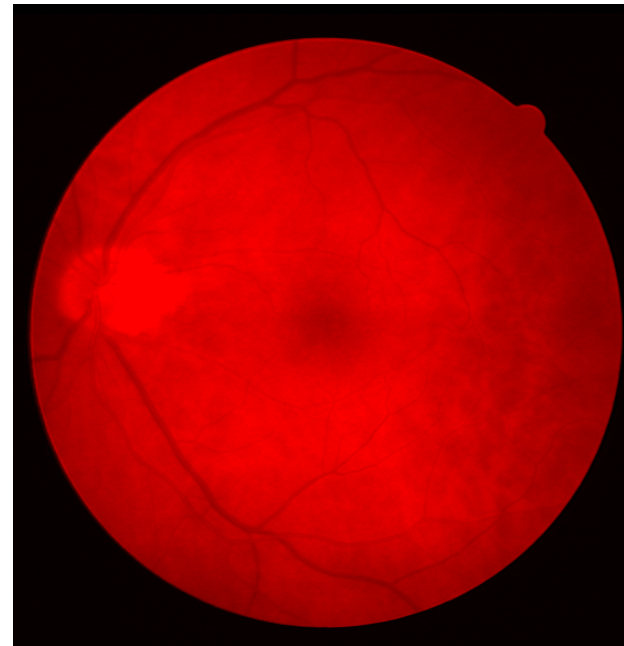
Selection of Color Image Components or Channels

- ❖ Gabor filters are sensitive to high-contrast features.
- ❖ Each color channel was analyzed in terms of blood vessel : background contrast.
- ❖ Luminance component Y of the YIQ model combines the three color channels (RGB): lower noise and higher contrast.

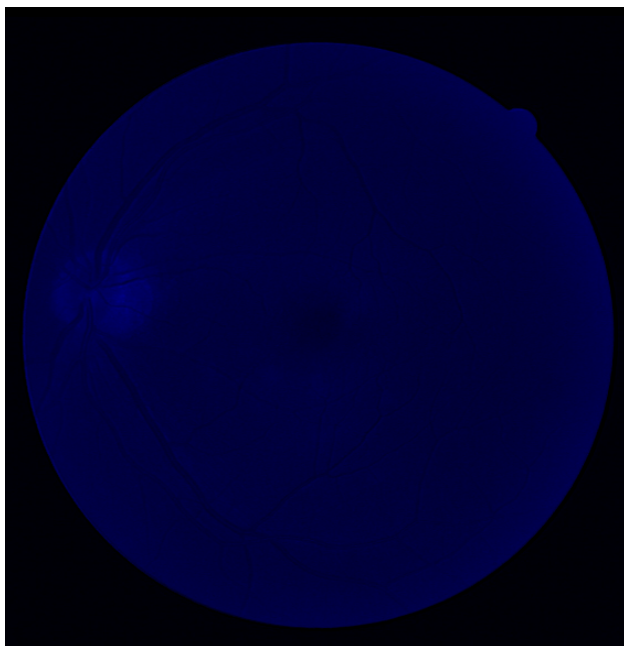
Original
RGB
color
image:
DRIVE
12



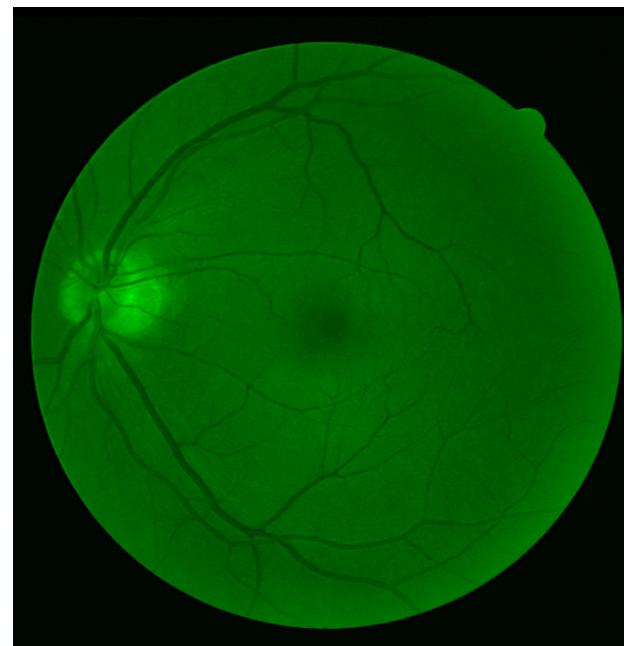
Red
channel



Blue
channel



Green channel



Inverted
 γ
channel



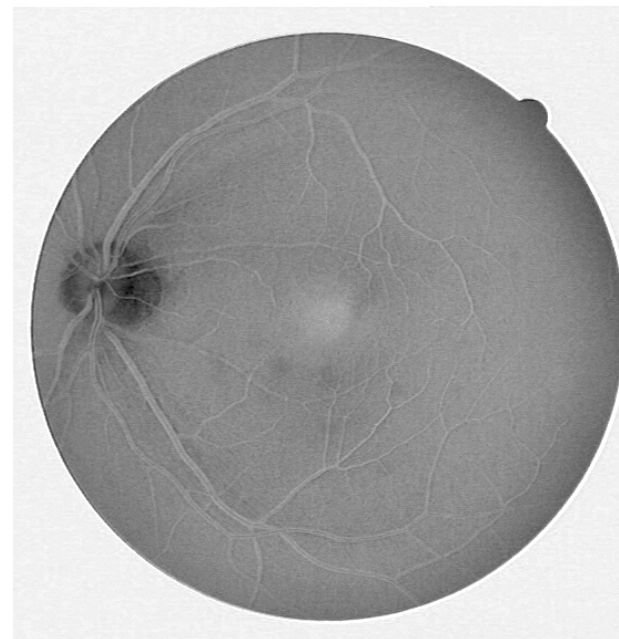
Inverted
red
channel



Inverted
green
channel



Inverted
blue
channel





Selection of Color Image Components or Channels

- ❖ The red & blue channels are noisy and are not suitable for the detection of blood vessels on their own.
- ❖ The inverted green channel has the highest contrast among the RGB channels.
- ❖ The blue and red channels contain useful information: higher contrast of vessels in the inverted γ channel.



Preprocessing of Color Images

- ❖ Each (red, green, blue) image was normalized to the range [0, 1].
- ❖ Luminance component Y of the YIQ model:
$$Y = 0.299 \text{ } R + 0.587 \text{ } G + 0.114 \text{ } B$$
- ❖ The inverted Y channel image was used.
- ❖ Effective region of each image obtained by thresholding the Y channel image at 0.1.



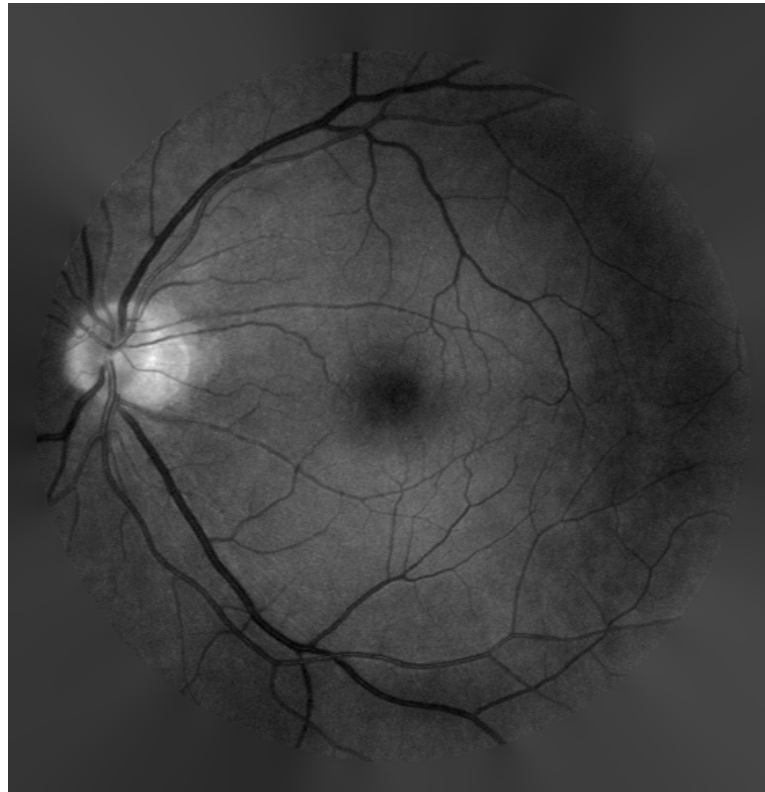
Preprocessing of Color Images

- ❖ Morphological erosion applied with a disc-shaped structuring element of diameter 10 pixels to remove edge artifacts.
- ❖ Pixels at the outer edge of the effective region identified using a four-pixel neighborhood.
- ❖ Each pixel replaced by the mean over a 21 X 21 neighborhood within the effective region.

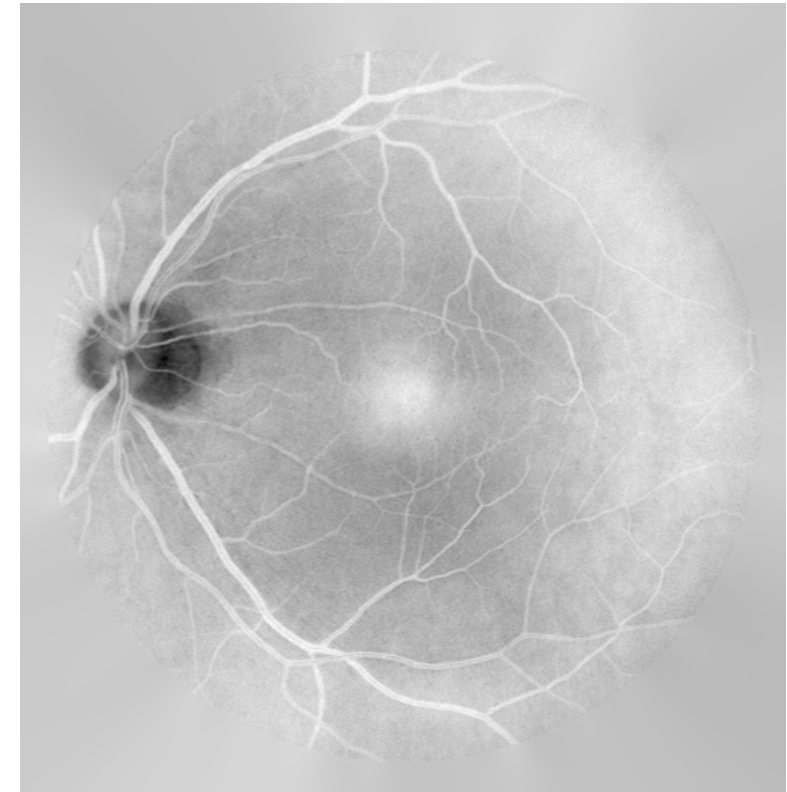


UNIVERSITY OF
CALGARY

Preprocessed Images



*Y component extended
beyond the effective area*



Inverted Y component



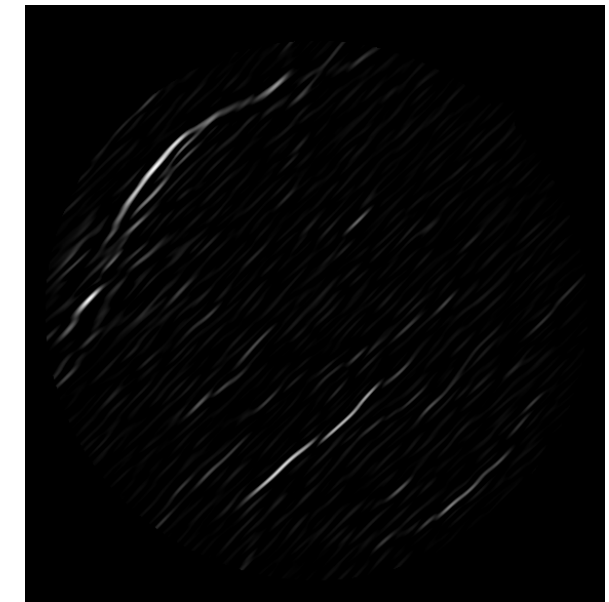
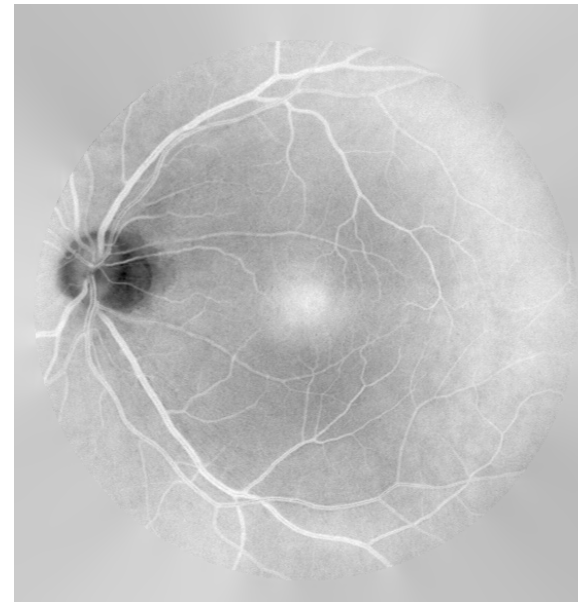
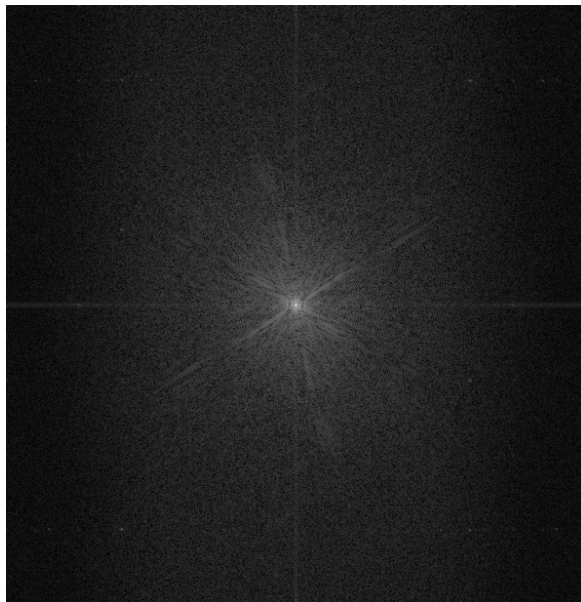
Gabor Filtering

- ❖ Gabor filters were applied to the inverted and preprocessed Y channel.
- ❖ A bank of 180 Gabor wavelets was used over the range of $[-90^\circ, 90^\circ]$.
- ❖ Parameters τ and l were varied over a large range to facilitate multiscale analysis and detection of curvilinear structures.



UNIVERSITY OF
CALGARY

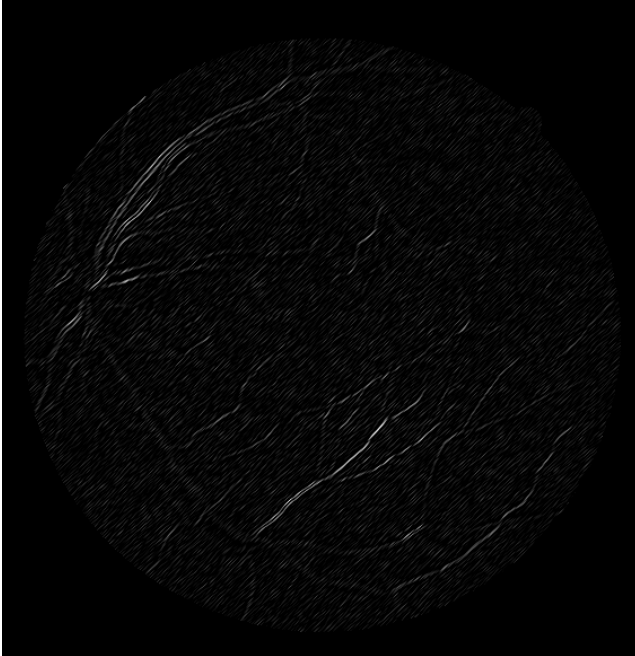
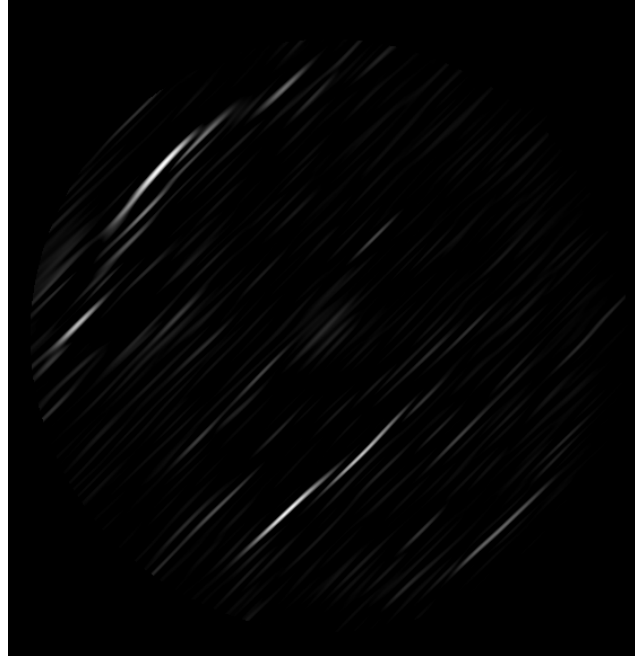
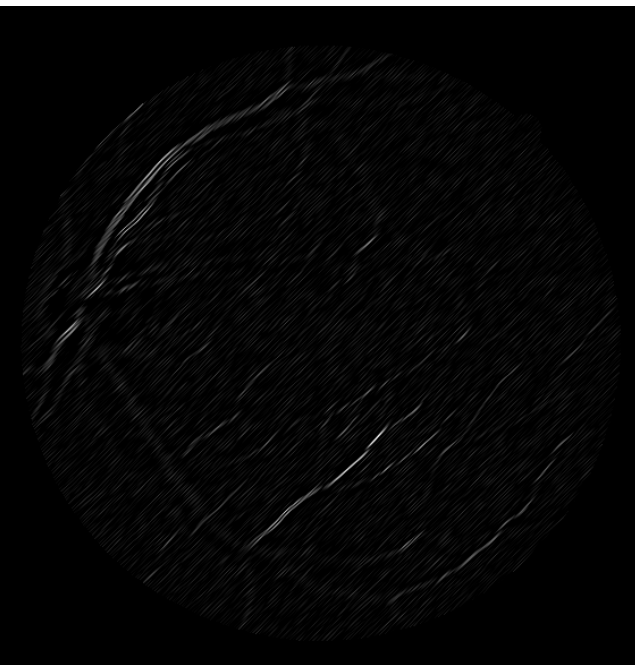
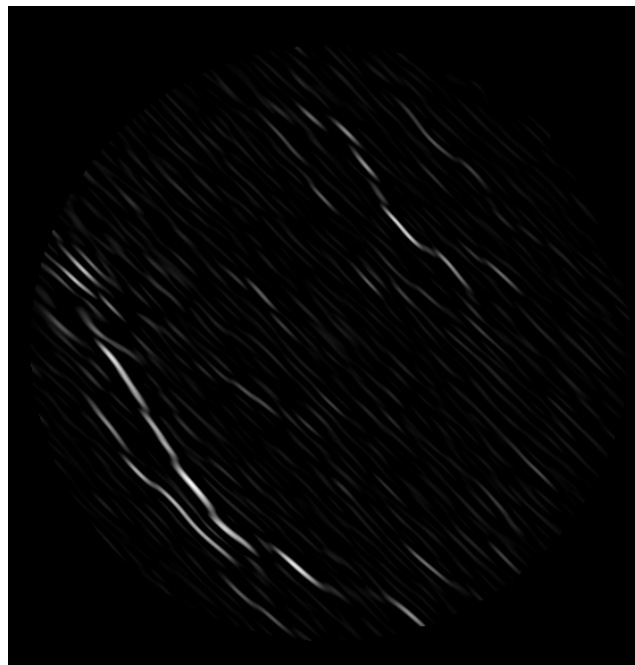
Results of Gabor Filtering



Log magnitude spectrum

Inverted Y channel

*Magnitude response of
a single Gabor wavelet:
 $\tau = 8, \lambda = 2.9, \theta = 45^\circ$*

$\tau = 2$
 $I = 2.9$
 $\theta = 45^\circ$  $\tau = 8$
 $I = 6$
 $\theta = 45^\circ$  $\tau = 2$
 $I = 6$
 $\theta = 45^\circ$  $\tau = 8$
 $I = 2.9$
 $\theta = -45^\circ$ 

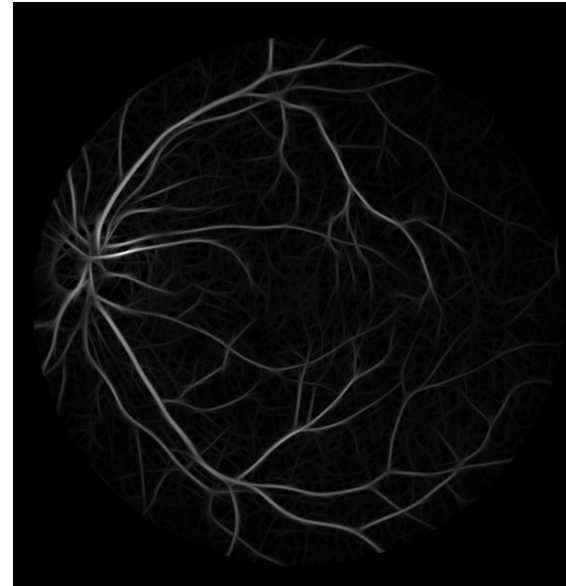


UNIVERSITY OF
CALGARY

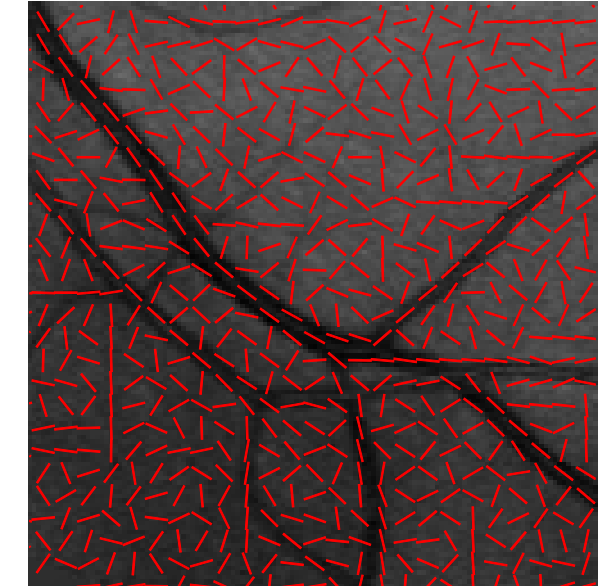
Results of Gabor Filtering



Original Image
 (584×565)



Gabor Magnitude
(max over 180 angles)

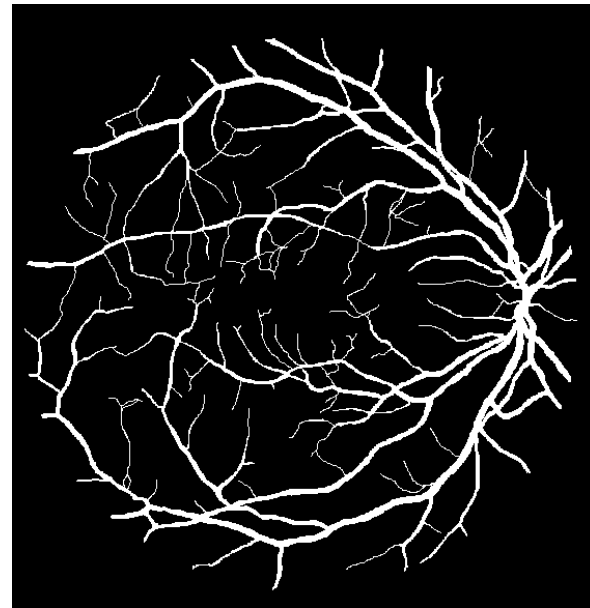


Gabor Angle

*Original
DRIVE
01*

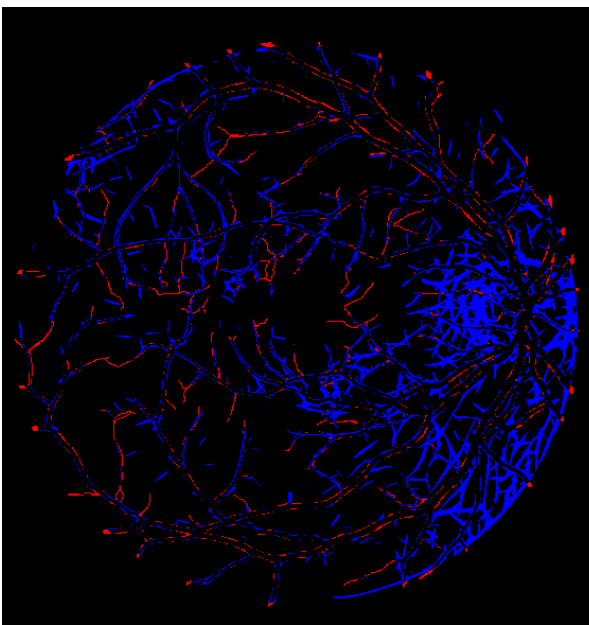


*Manual
labeling*

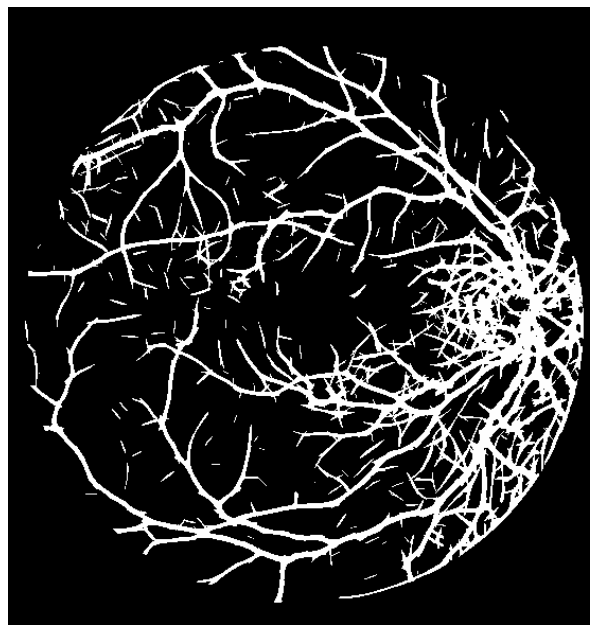


*Blue: false
positive*

*Red: false
negative*



*Result
of
detect-
ion*





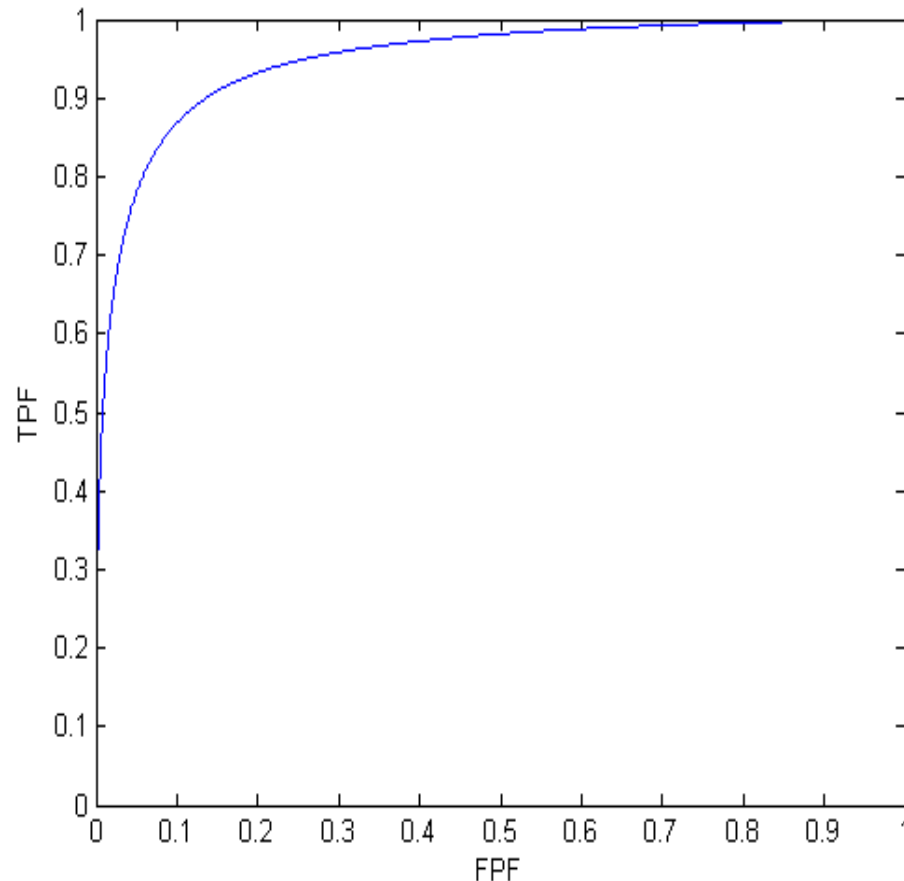
Results: ROC A_z for 20 Images using the *Y Channel*

Parameters	$l = 1.7$	2.1	2.5	2.9	3.3	3.7
$\tau = 1$	0.62	0.65	0.67	0.70	0.73	0.75
$\tau = 2$	0.69	0.72	0.75	0.77	0.79	0.81
$\tau = 4$	0.85	0.87	0.89	0.90	0.91	0.92
$\tau = 6$	0.91	0.92	0.93	0.94	0.94	0.94
$\tau = 7$	0.92	0.93	0.94	0.94	0.94	0.94
$\tau = 8$	0.93	0.94	0.94	0.94	0.94	0.94
$\tau = 9$	0.94	0.94	0.94	0.94	0.94	0.93
$\tau = 10$	0.94	0.94	0.94	0.93	0.93	0.92

ROC : Receiver Operating Characteristics
A_z : Area under the ROC curve



Results: ROC Curve for the DRIVE Test Set



$$\tau = 8, \quad I = 2.9, \quad A_z = 0.94$$



Multifeature Analysis

- ❖ To improve the single-scale classification results, other features representing different characteristics of the vessels were derived.
- ❖ Coherence is one of the features derived.
- ❖ Because blood vessels have high contrast in the **green** channel, the inverted green channel was used as a feature.



Coherence

- ❖ Coherence is a measure of the strength of orientation or anisotropy.

$$\gamma_{pq} = G_{pq} \frac{\sum_{m=1}^P \sum_{n=1}^P |G_{mn} \cos(\theta_{mn} - \psi_{pq})|}{\sum_{m=1}^P \sum_{n=1}^P G_{mn}}$$

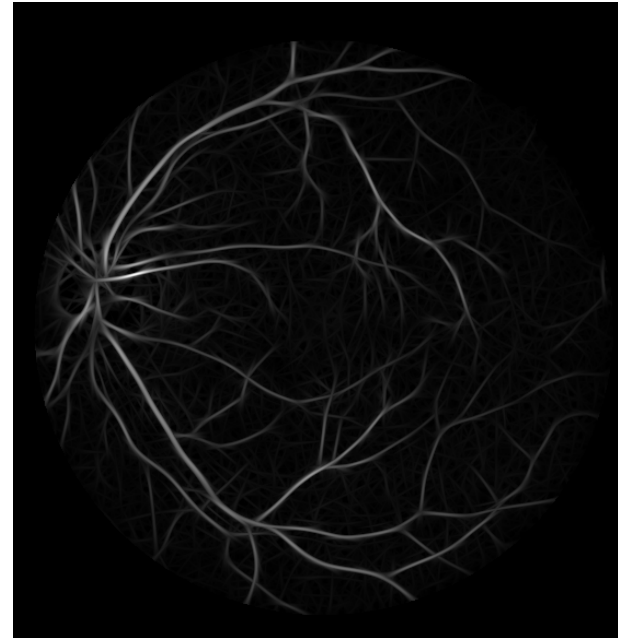
G_{mn} : gradient magnitude,
 θ_{mn} : gradient orientation,
 ψ_{pq} : local orientation.

$$\psi_{pq} = \frac{1}{2} \arctan \frac{\sum_{m=1}^P \sum_{n=1}^P G_{mn}^2 \sin(2\theta_{mn})}{\sum_{m=1}^P \sum_{n=1}^P G_{mn}^2 \cos(2\theta_{mn})} + \frac{\pi}{2}$$

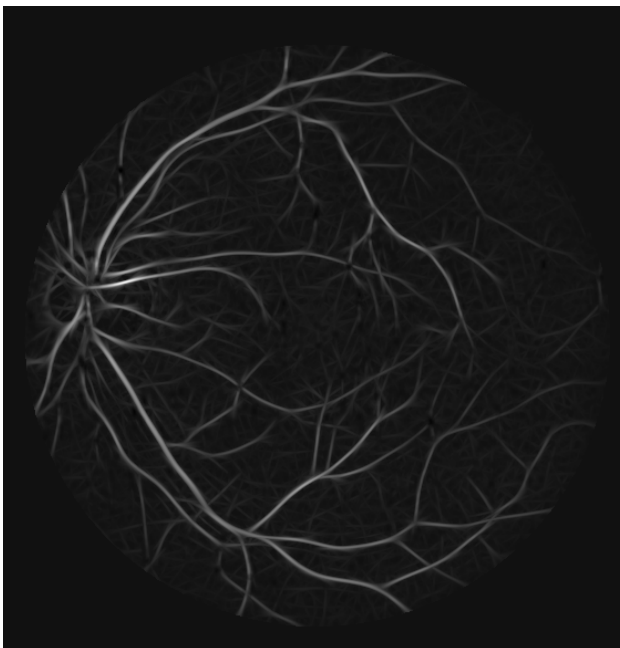
Original
Image



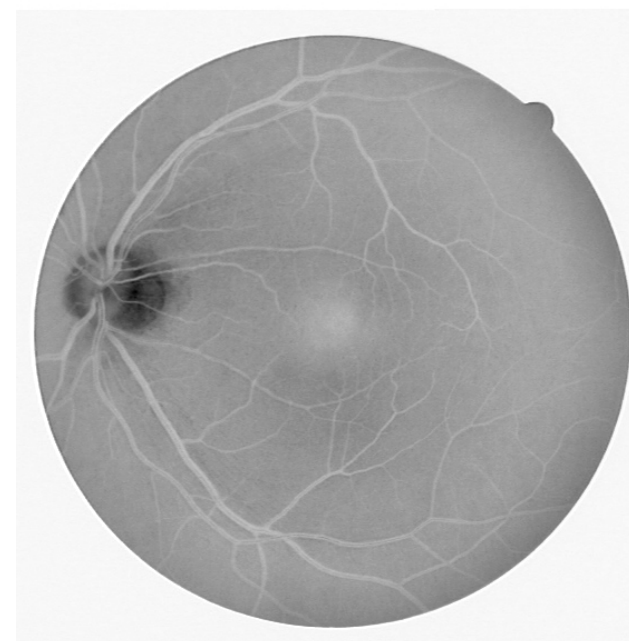
Gabor
magnitude



Coherence



Inverted
green
channel





Multifeature Analysis and Classification

- ❖ Training and testing of the three features (Gabor magnitude, coherence, green channel) was done using various classifiers:
 - Single-layer Perceptron (SLP):
single-layer feed-forward (SLFF)
artificial neural network (ANN).
 - Multilayered Perceptron (MLP).
 - Radial Basis Functions (RBF).



Results of Multifeature Analysis

Classification Method	A_z
Coherence only	0.8215
SLP (Gabor Magnitude and Coherence) with 10 nodes using 50% of the training data	0.9508
MLP (Gabor Magnitude and Coherence) with 2 layers (3 nodes and 1 node) using 50% of the training data	0.9507
MLP (Gabor Magnitude and Green) with 2 layers (3 nodes and 1 node) using 50% of the training data	0.9456
RBF (Gabor Magnitude and Coherence) with sigma=1.2 using 0.125% of the training data	0.9516



Results with Different Input Images

Input Image	Gabor Parameters	A_z
Y of YIQ color space	$\tau = 8, I = 2.9, K = 180$	0.9418
Green channel	$\tau = 8, I = 2.9, K = 180$	0.9397
0.2 * R + 0.8 * G	$\tau = 8, I = 2.9, K = 180$	0.9402

Multiscale Gabor Filtering

- ❖ Vessels in the retina vary in thickness: 50 to 200 μm .
- ❖ The parameters of the Gabor filter (τ, I) may be varied to detect vessels at different scales of thickness and elongation.
- ❖ Various combinations of scales were used for multiscale analysis.



Multiscale Analysis

1. Maximum Gabor response over all scales
2. Classifiers:
 - I. Generic Multilayer Perceptron:
 - 2 or 3 layers
 - Using the discriminant function (tan-sig)
 - Using 10% of training data
 - II. Radial Basis Functions:
 - 8 or 15 nodes
 - Sigma fixed at 1.2
 - Used 0.125% of training data



Results of Multiscale Analysis

Classifier	# Layers	# Nodes per layer	Scales	A _z
MLP	2	20, 1	$\tau = 8, 12$	0.9522
MLP	2	20, 1	$\tau = 1, 4, 8$	0.9554
MLP	2	20, 1	$\tau = 4, 8, 12$	0.9592
MLP	3	20, 20, 1	$\tau = 0.5, 4, 8, 12$	0.9587
MLP	3	30, 30, 1	$\tau = 4, 8, 12$	0.9596

Classifier	# Nodes	Scales	A _z
RBF	8	$\tau = 4, 8, 12$	0.9572
RBF	15	$\tau = 4, 8, 12$	0.9565
RBF	8	$\tau = 0.5, 4, 8, 12$	0.9565
RBF	8	$\tau = 1, 4, 8, 12$	0.9547



Comparative Analysis with Other Works

Detection method	A_z
Matched filter; Chaudhuri et al.	0.91
Adaptive local thresholding; Jiang and Mojon	0.93
Ridge-based segmentation; Staal et al.	0.95
Single-scale Gabor filters; Rangayyan et al.	0.95
Multiscale Gabor filters; Soares et al.	0.96
Multiscale Gabor filters; present work	0.96

A_z values with 20 test images from DRIVE



Comparative Analysis

Our results closely match those of Soares et al.

Major differences:

1. Real instead of complex Gabor functions.
2. Simple MLP not assuming a Gaussian mixture model.
3. Luminance component instead of the green channel of the color fundus images: noise reduced.



Remarks

- ❖ Multiscale Gabor wavelets provide high efficiency in the detection of retinal blood vessels.
- ❖ The proposed methods could assist in the diagnosis of various pathologies and localization of features.
- ❖ Methods need to be developed to address the large number of false-positive pixels around the ONH.
- ❖ Methods need be developed for optimal use of the information in the various color components.

Detection of the Optic Nerve Head in Fundus Images of the Retina

Xiaolu Iris Zhu, Rangaraj M. Rangayyan,
Fábio J. Ayres, and Anna L. Ells

Department of Electrical and Computer Engineering,
Schulich School of Engineering, University of Calgary
Division of Ophthalmology, Alberta Children's Hospital
Calgary, Alberta, Canada



UNIVERSITY OF
CALGARY

SCHULICH
School of Engineering



DEPARTMENT OF ELECTRICAL
AND COMPUTER ENGINEERING



The Optic Nerve Head

Need for the detection
of the ONH:

- ❖ Important anatomical feature (landmark).
- ❖ Computer-assisted diagnosis.
- ❖ A step in the early detection of retinal pathology.



DRIVE image 01
(584×565 pixels)



Objectives

- ❖ Locate the approximate boundary of the ONH based on its circularity.
- ❖ Locate the center of the ONH as the point of convergence of the main blood vessels.



Detection of the ONH using the Hough Transform

Detect edges

- ❖ Sobel operators or Canny method

Detect circles

- ❖ Hough transform for the detection of circles

Select circle

- ❖ Use intensity criterion to select the best-fitting circle for the ONH



Detection of Edges

- ❖ Sobel Operators:

$$\begin{bmatrix} -1 & -2 & -1 \\ 0 & 0 & 0 \\ 1 & 2 & 1 \end{bmatrix} \quad \begin{bmatrix} -1 & 0 & 1 \\ -2 & 0 & 2 \\ -1 & 0 & 1 \end{bmatrix}$$

- Combined gradient magnitude:

$$|\mathbf{G}(x,y)| = [G_x^2(x,y) + G_y^2(x,y)]^{1/2}$$

- ❖ Canny Method

- ❖ Apply a threshold to obtain an edge map.



Detection of Circles: The Hough Transform

- ❖ The points lying on the circle

$$(x - a)^2 + (y - b)^2 = c^2$$

are represented by a single point in the 3D parameter space (a, b, c)

- ❖ Hough space: accumulator $A(a, b, c)$

Procedure to Detect Circles

1. Obtain a binary edge map of the preprocessed Y channel image.
2. Set ranges for a and b .
3. Solve for the value of c that satisfies
$$(x - a)^2 + (y - b)^2 = c^2.$$
4. Update the accumulator corresponding to (a, b, c) .
5. Update values for a and b within the range of interest and go back to Step 3.

Set Up of the Hough Space

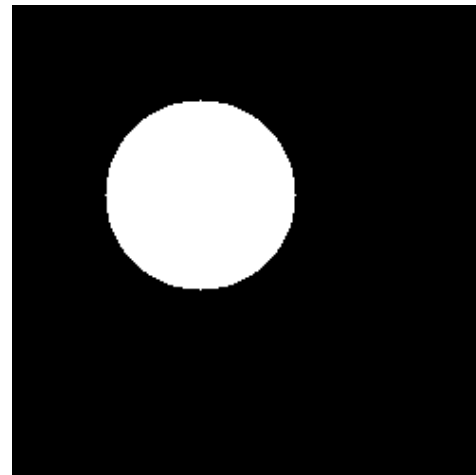
- ❖ Average diameter of the ONH: 1.5 mm.
- ❖ Radius of a circular approximation to the ONH: 600 to 1000 μm .
- ❖ Spatial resolution of the DRIVE images: 20 μm per pixel.
- ❖ Range for the radius c : 31 to 50 pixels.
- ❖ Size of the Hough space: $584 \times 565 \times 20$.



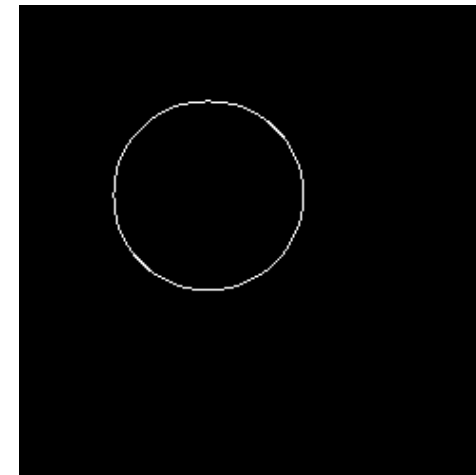
UNIVERSITY OF
CALGARY

Detection of Circles

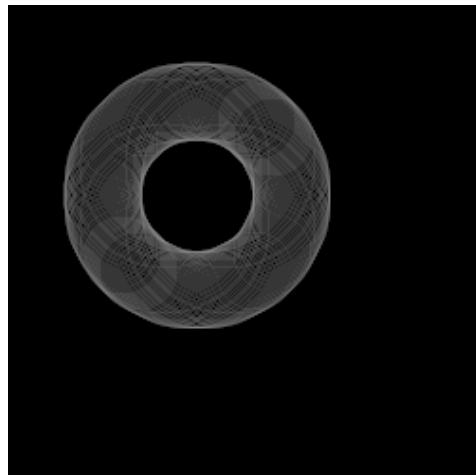
*Original
image*



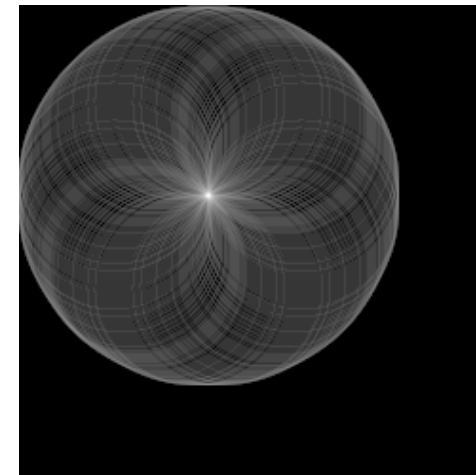
*Edge
map*



*Hough
space
 $c = 20$*



*Hough
space
 $c = 50$*

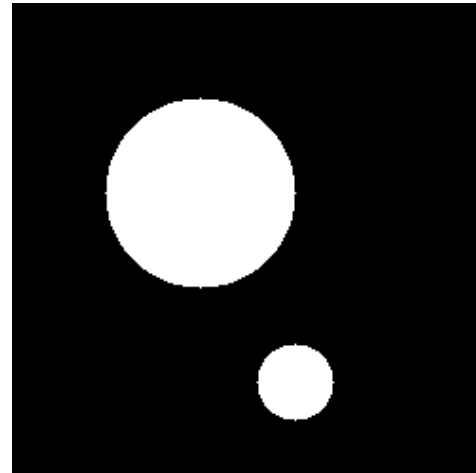




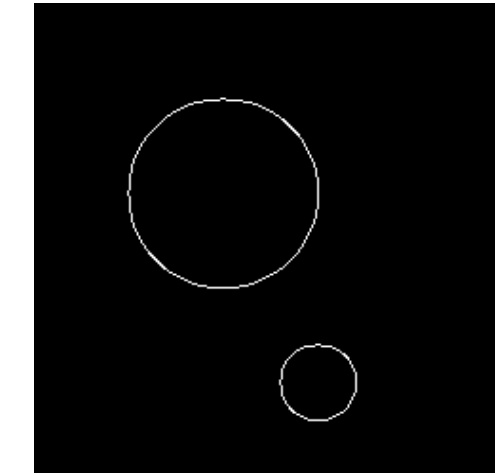
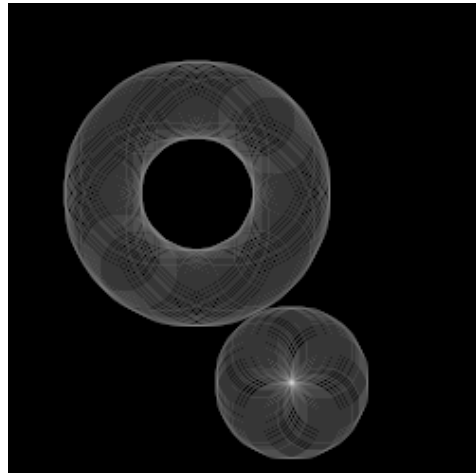
UNIVERSITY OF
CALGARY

Detection of Circles

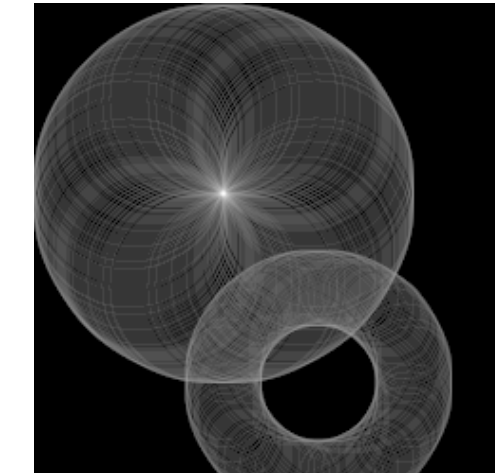
*Original
image*



*Hough
space
 $c = 20$*



*Edge
map*

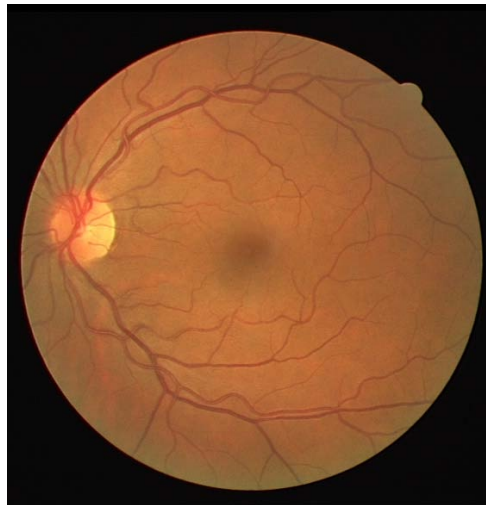


*Hough
space
 $c = 50$*

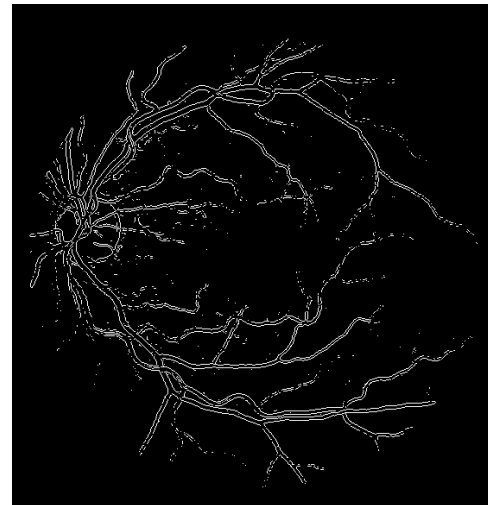


UNIVERSITY OF
CALGARY

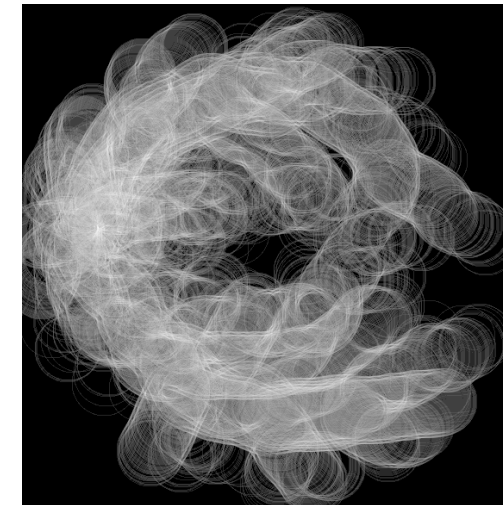
Detection of Circles



DRIVE image 01
 584×565 pixels



Edge map
using
Sobel
operators

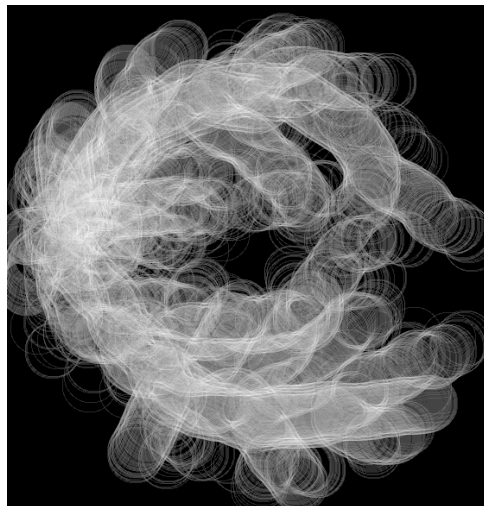


Hough
space
 $c = 37$ pixels

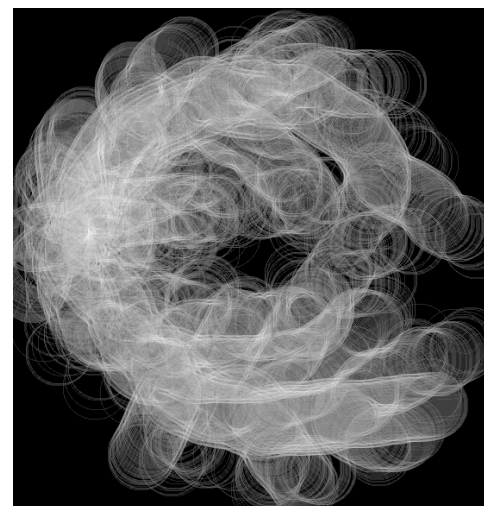


UNIVERSITY OF
CALGARY

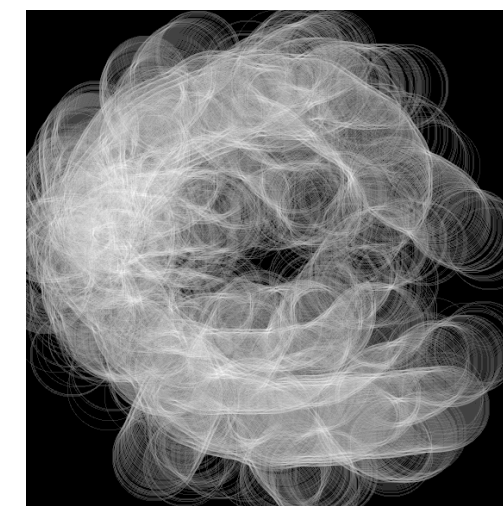
Hough-space Planes



$c=31$ pixels



$c=37$ pixels



$c=47$ pixels



Detection of the ONH

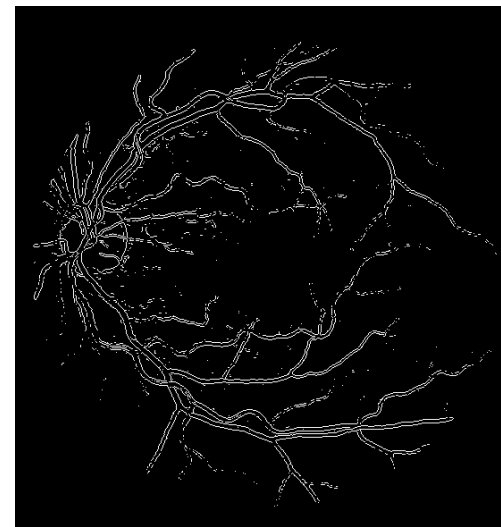
- ❖ Check each of the top 30 potential circles indicated by the local maxima (peaks) in the Hough transform to verify if it could represent the ONH using a fraction of the reference intensity:
90% of the maximum intensity of the Y channel for the given image (DRIVE and STARE databases).



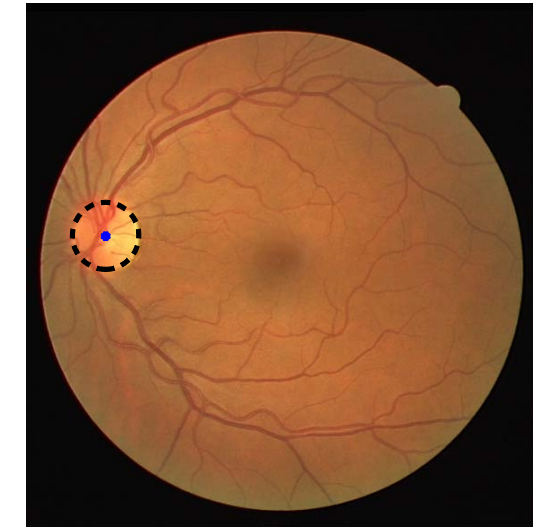
Results



DRIVE image 01



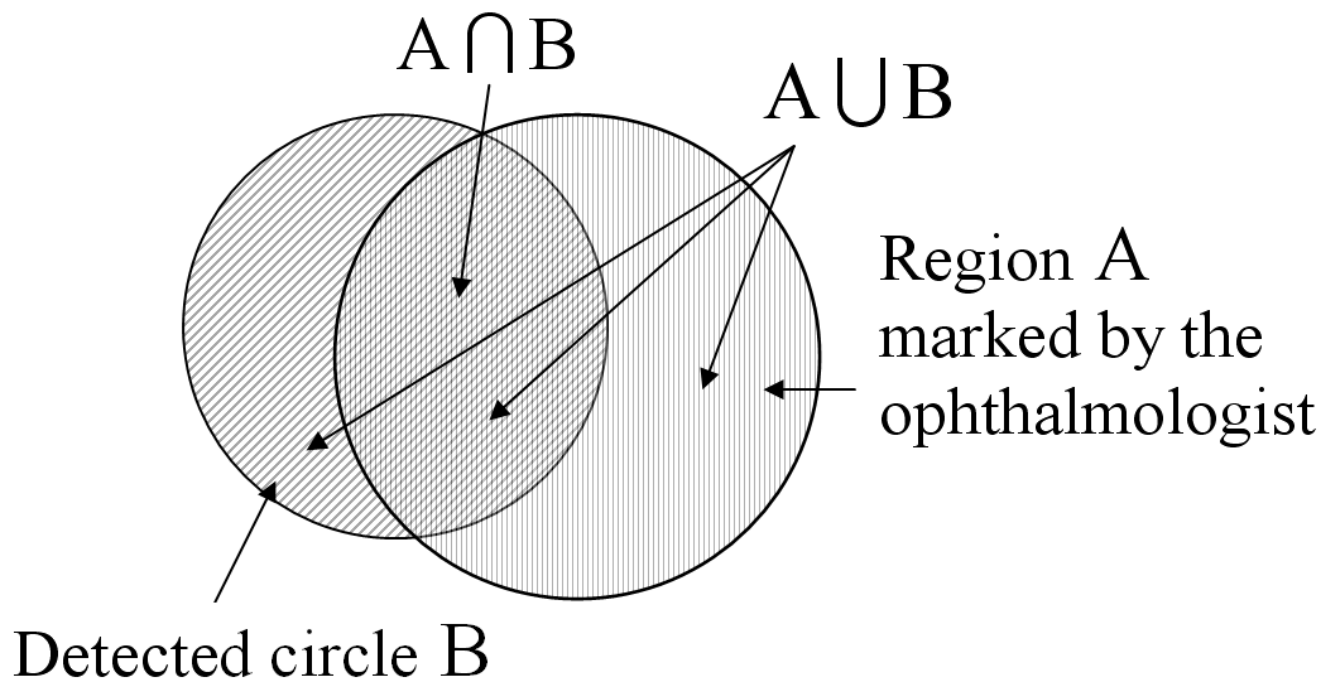
Edge map
using Sobel
operators



Successfully
detected
ONH



Measure of Performance: Overlap





Results: 40 DRIVE Images

Distance: between the detected center and the center marked by an ophthalmologist.

Overlap: ratio of the intersection of the detected circular region and the ONH delineated by the ophthalmologist to their union.

Method	Distance mm (pixels)		Overlap	
	mean	std	mean	std
First peak in the Hough space	1.05 (52.5)	1.87 (93.5)	0.58	0.36
Peak selected using intensity condition	0.36 (18)	1.00 (50)	0.73	0.25



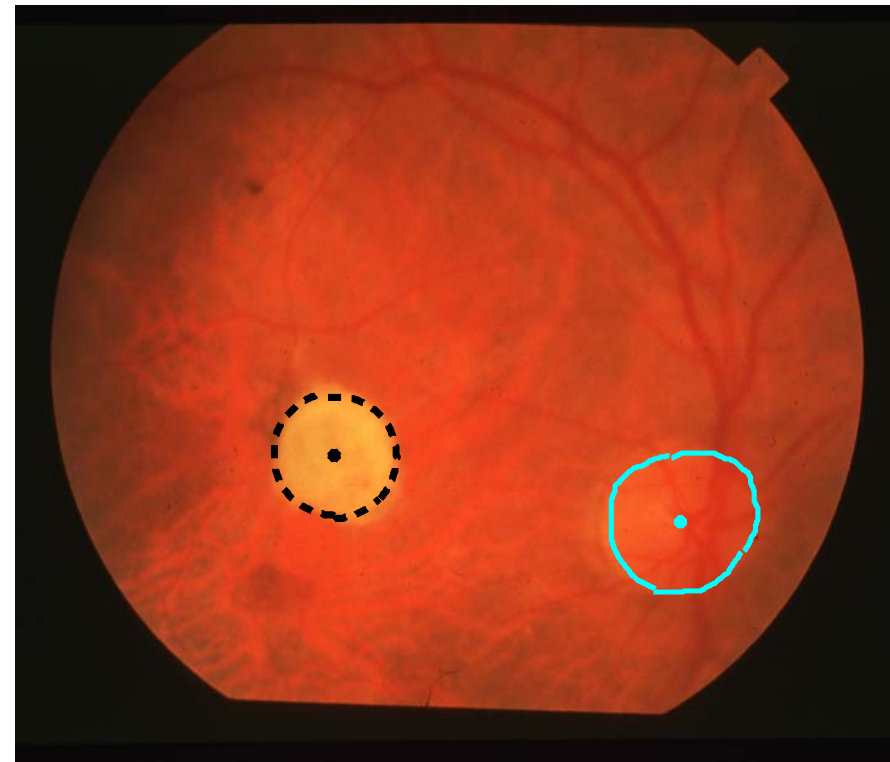
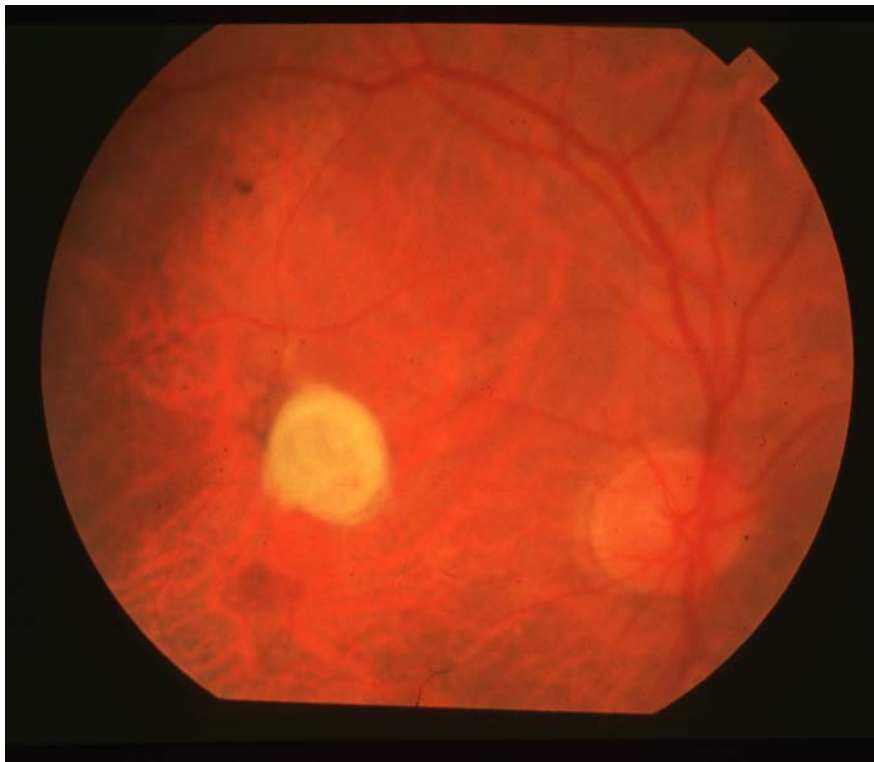
Results: 81 STARE Images

Method	Distance (pixels)		Overlap	
	Mean	std	mean	std
First peak in the Hough space	150.5	140.5	0.21	0.27
Peak selected using intensity condition	132.5	159	0.32	0.30



UNIVERSITY OF
CALGARY

ONH Missed: STARE im0036





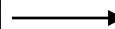
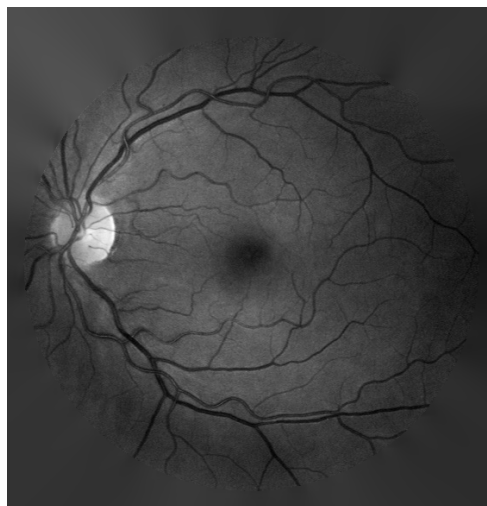
Detection of the ONH as the Convergence of Blood Vessels

1. Extract the orientation field using Gabor filters.
2. Filter and down-sample the orientation field.
3. Analyze the orientation field using phase portraits.
4. Post-process the phase portrait maps.
5. Detect sites of convergence of blood vessels.
6. Select the point of convergence to represent the center of the ONH.

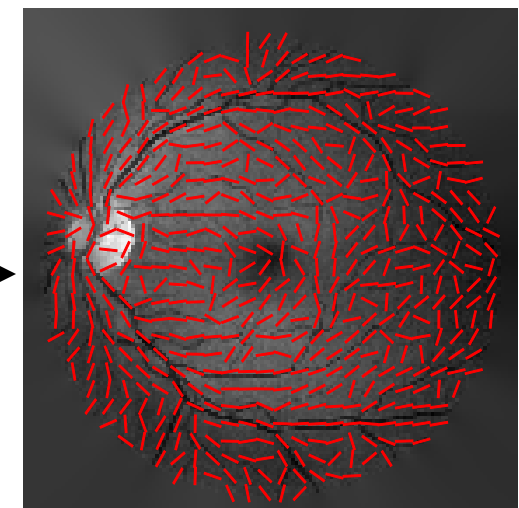


Extract the Orientation Field

- ❖ Compute the texture orientation (angle) for each pixel with $\lambda = 2.9$, $\tau = 8$ pixels.

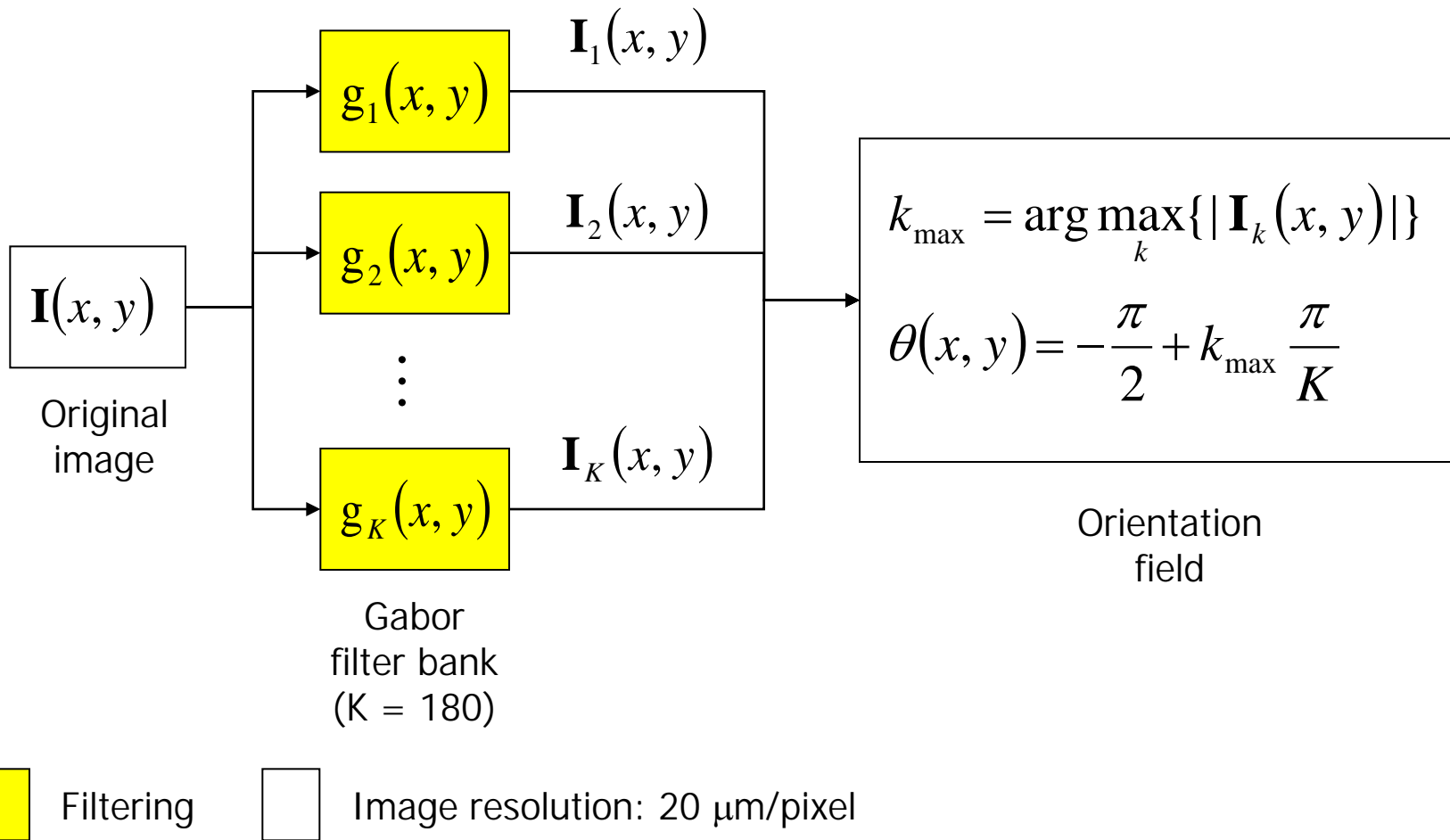


Gabor filtering
(line detection)





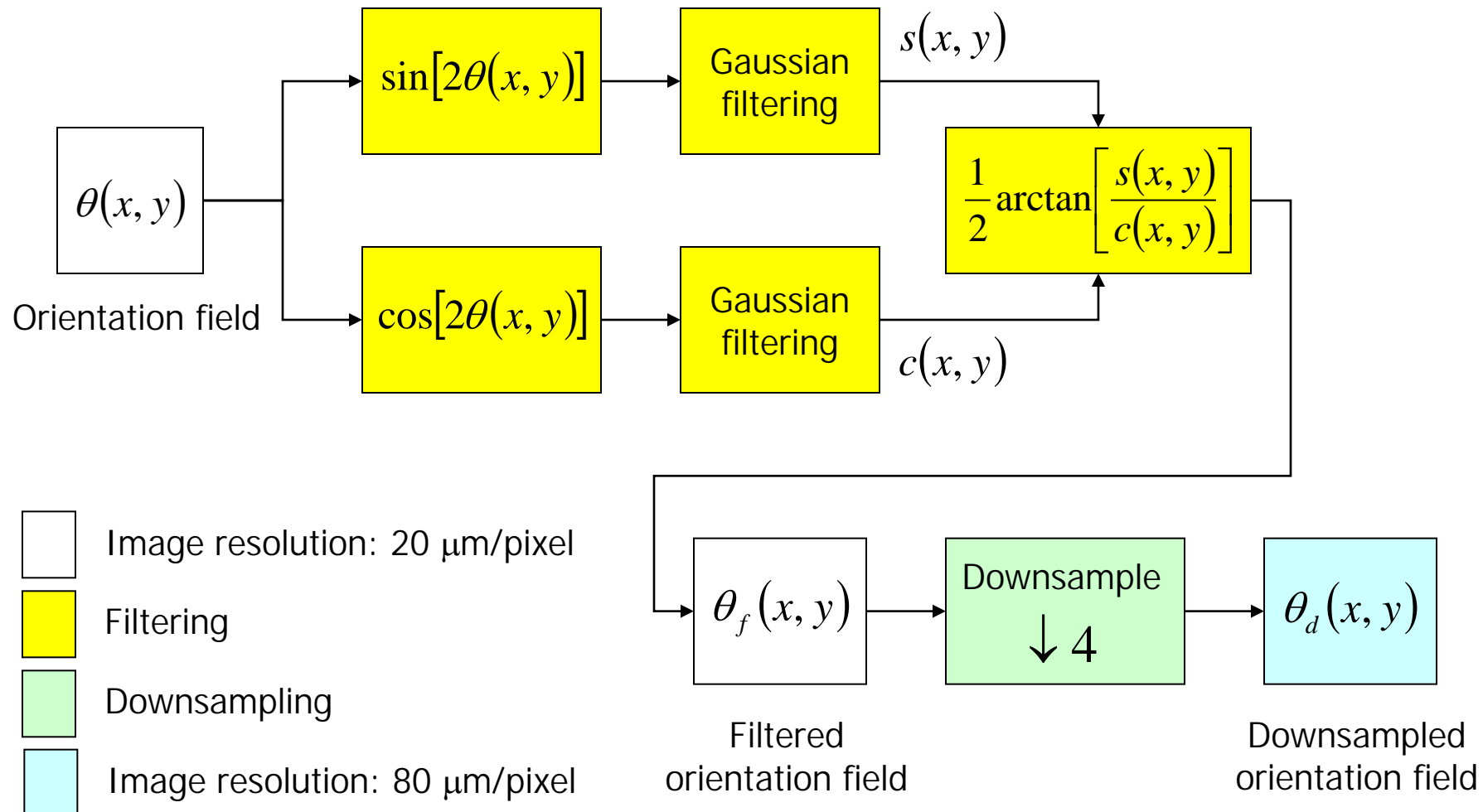
Extracting the Orientation Field





UNIVERSITY OF
CALGARY

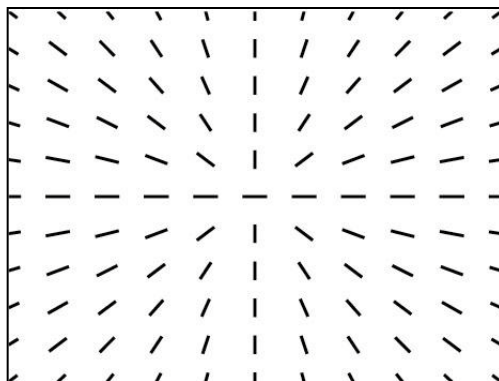
Filtering and Down-sampling the Orientation Field



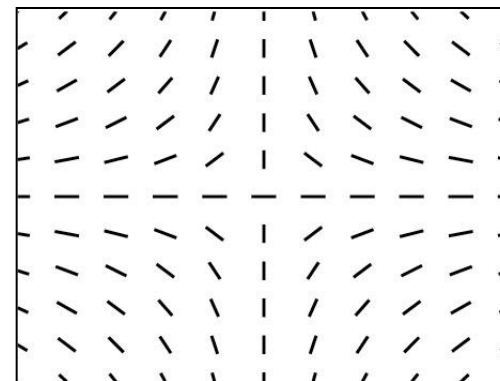


Phase Portraits

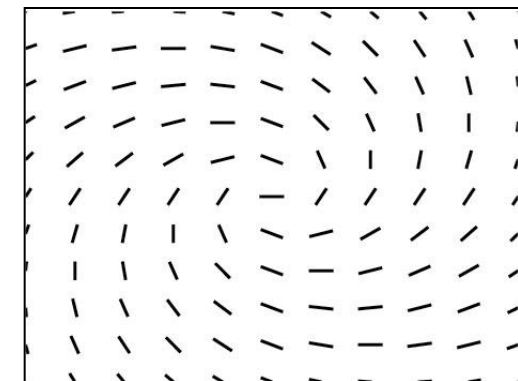
$$\vec{v}(x, y) = \begin{pmatrix} v_x \\ v_y \end{pmatrix} = \mathbf{A} \begin{pmatrix} x \\ y \end{pmatrix} + \mathbf{b}, \quad \mathbf{A} = \begin{bmatrix} a & b \\ b & c \end{bmatrix}, \quad \mathbf{b} = \begin{bmatrix} d \\ e \end{bmatrix}$$



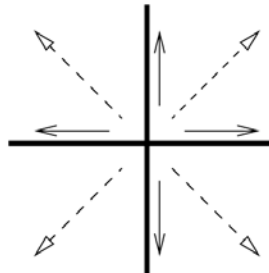
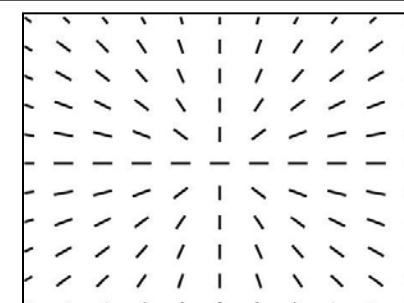
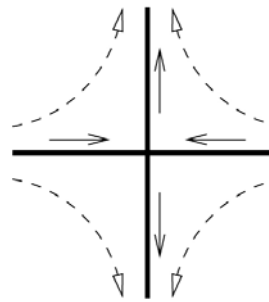
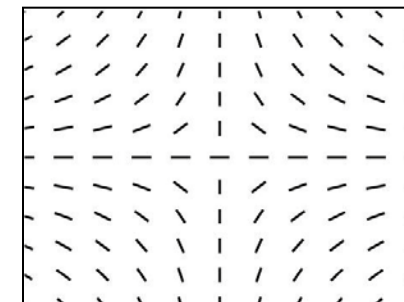
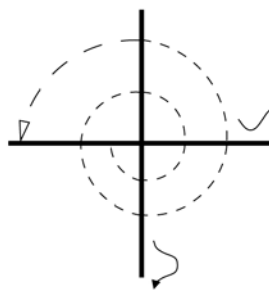
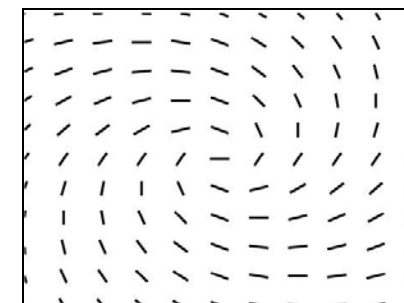
node



saddle



spiral

Phase portrait type	Eigenvalues of matrix A	Streamlines	Orientation field
Node	Real, same sign		
Saddle	Real, opposite sign		
Spiral	Complex conjugate		



UNIVERSITY OF
CALGARY

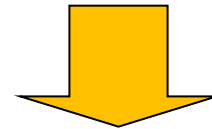
Model Error

Orientation field

$$\theta(x, y)$$

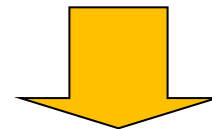
Model-generated field

$$\phi(x, y | \mathbf{A}, \mathbf{b})$$



$$\Delta(x, y) = \sin[\theta(x, y) - \phi(x, y | \mathbf{A}, \mathbf{b})]$$

Local error measure



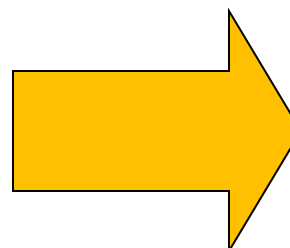
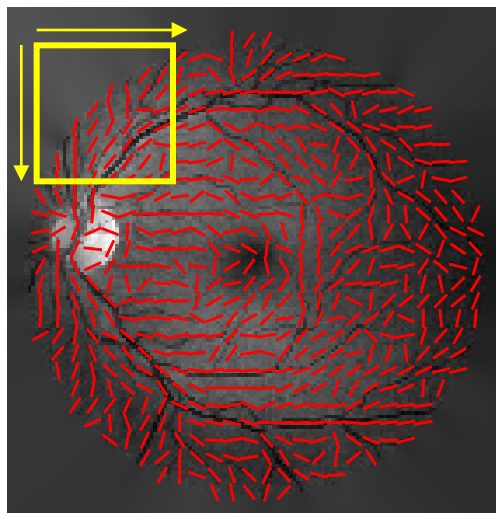
$$\varepsilon^2(\mathbf{A}, \mathbf{b}) = \sum_x \sum_y \Delta^2(x, y)$$

Sum of the squared
error measure



Phase Portrait Analysis (step 1 of 3)

1. Fit phase portrait model to the analysis window



$$\mathbf{A} = \begin{bmatrix} 1.1 & 0.3 \\ -0.2 & 1.7 \end{bmatrix}$$

$$\mathbf{b} = \begin{bmatrix} -4.8 \\ -7.9 \end{bmatrix}$$

Window size:
 40×40 pixels

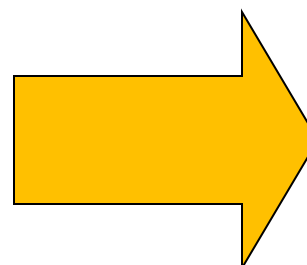


Phase Portrait Analysis (step 2 of 3)

2. Find optimal phase portrait type and location of fixed point

$$A = \begin{bmatrix} 1.1 & 0.3 \\ -0.2 & 1.7 \end{bmatrix}$$

$$b = \begin{bmatrix} -4.8 \\ -7.9 \end{bmatrix}$$



Type: node

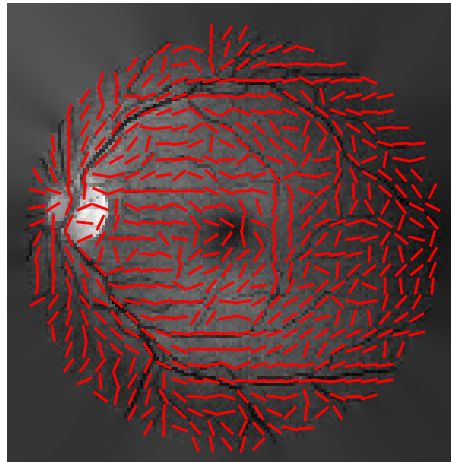
$$X = \begin{bmatrix} x \\ y \end{bmatrix} = -A^{-1}b$$

Fixed point:
 $x=3, y=5$

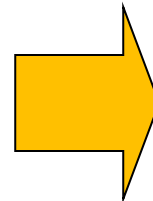


Phase Portrait Analysis *(step 3 of 3)*

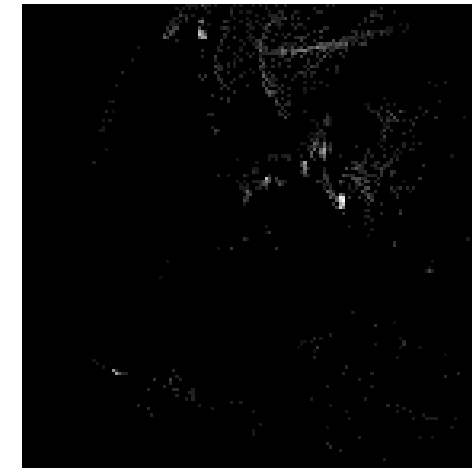
3. Cast a vote in the corresponding phase portrait map



Orientation
field



Log (1 + Node)
[0, 1.526]



Log (1 + Saddle)
[0, 1.576]



Detection of the Center of the ONH

- ❖ Check each peak in the node map to verify if it could represent the center of the ONH using a fraction of the reference intensity.

- ❖ Fraction = 68% for the DRIVE images.
- ❖ Fraction = 50% for the STARE images.



UNIVERSITY OF
CALGARY

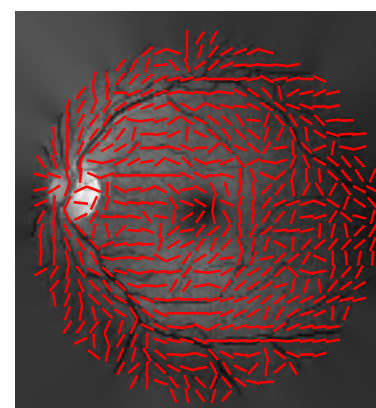
Results of Detection of the Center of the ONH



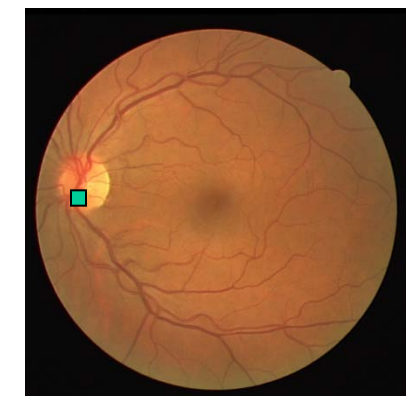
DRIVE
Image 01



Magnitude
response of
the Gabor
filters



Orientation
field

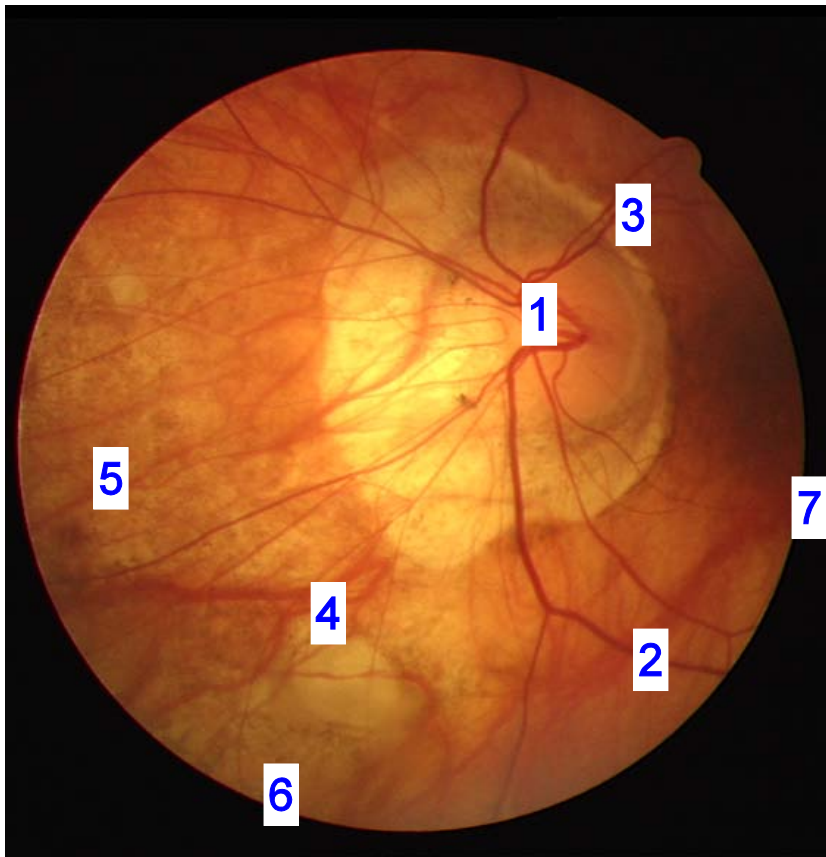


Successfully
detected ONH

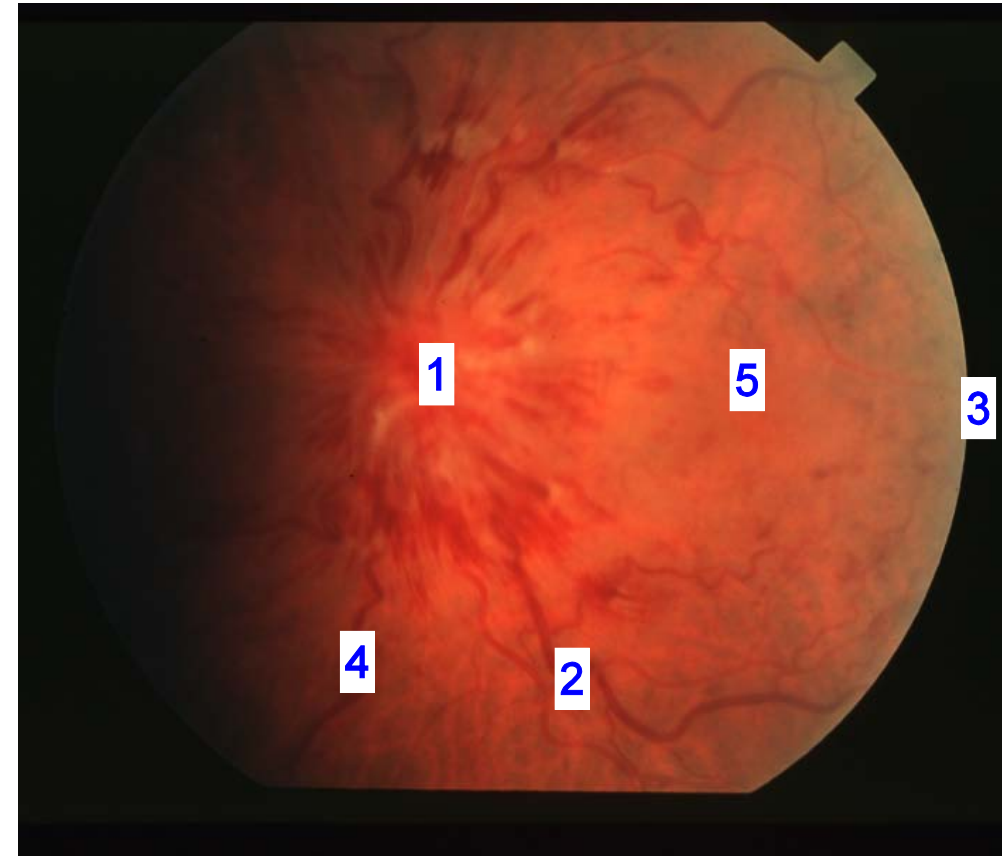


UNIVERSITY OF
CALGARY

Successful Detection with Difficult Images



DRIVE 34



STARE im0021



UNIVERSITY OF
CALGARY

Results of Detection of the Center of the ONH



STARE image im0139
(700×605 pixels),
distance = 321 pixels

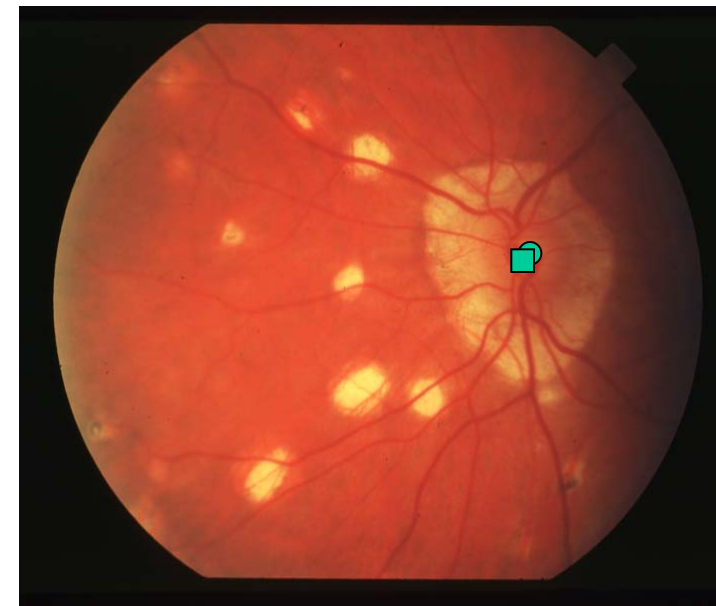


Image im0010,
distance = 2.2 pixels



Results of Detection of the Center of the ONH

Statistics for the 40 images in the DRIVE database.

Method	Distance mm (pixels)	
	mean	std
First peak in node map	1.61 (80.7)	2.40 (120)
Peak selected using intensity condition	0.46 (23.2)	0.21 (10.4)



Results of Detection of the Center of the ONH

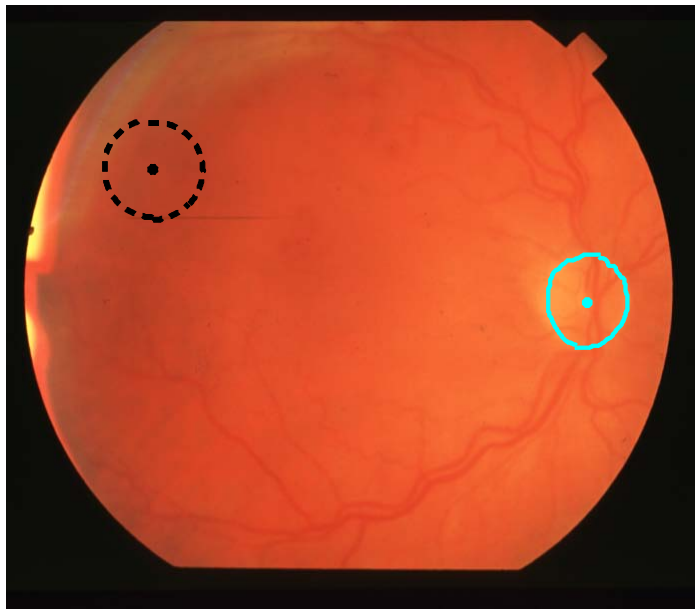
Statistics for the 81 images in the STARE database.

Method	Distance (pixels)	
	mean	std
First peak in node map	119	156
Peak selected using intensity condition	119	156

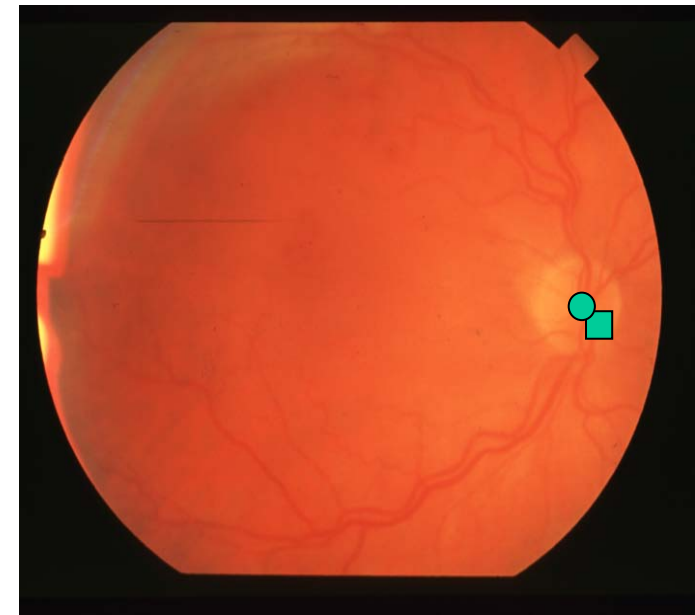


UNIVERSITY OF
CALGARY

Results of Detection of the ONH



STARE image im0035
(Hough transform),
distance = 454 pixels.
Result not acceptable.

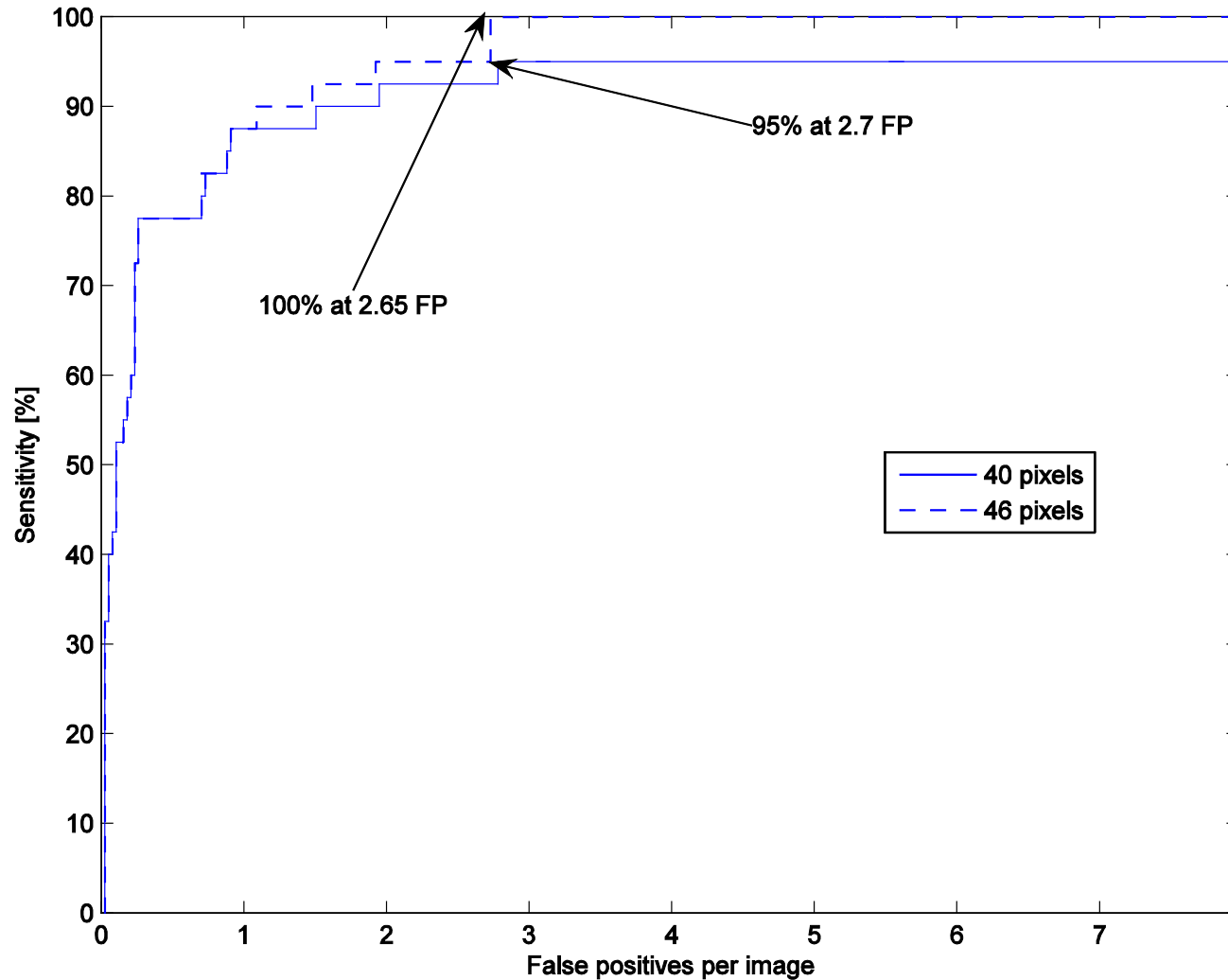


Phase portraits,
distance = 26 pixels.
Good result.



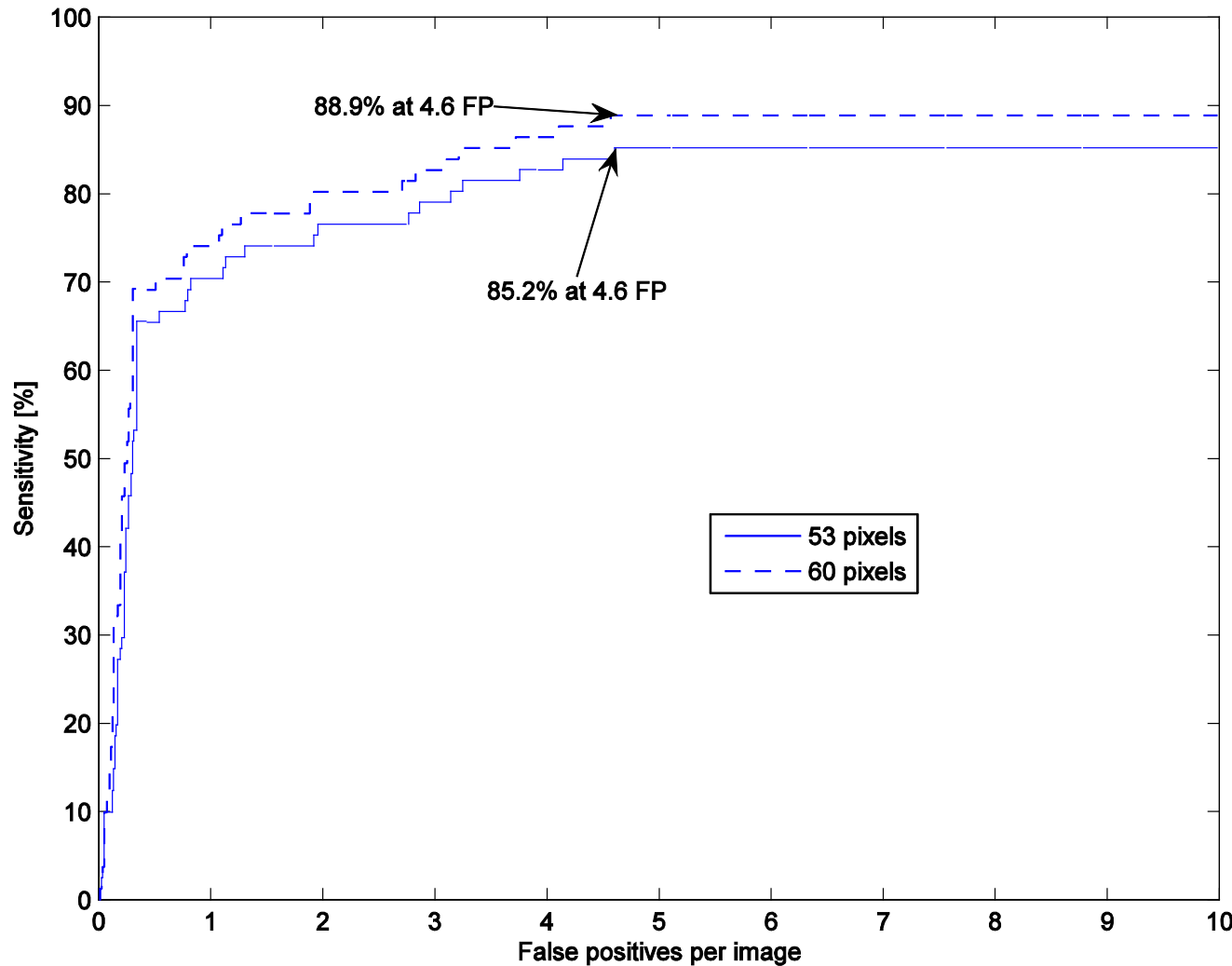
UNIVERSITY OF
CALGARY

Free-response Receiver Operating Characteristics: 40 images of DRIVE





Free-response Receiver Operating Characteristics: 81 images of STARE





Comparison of the Efficiency in Locating the ONH

Method of detection	DRIVE	STARE
Hoover and Goldbaum (fuzzy convergence)	-	89%
Foracchia et al. (geometrical model)	-	97.5%
Ter Haar (directional model)	-	93.8%
Park et al. (property-based)	90.3%	-
Ying et al. (fractal-based)	97.5%	-
Park et al. (tensor voting)	-	91.1%
Youssif et al. (matched filter)	100%	98.8%
Present work (Hough transform)	90%	44.4%
Present work (phase portraits)	100%	69.1%



Remarks

- ❖ Two methods based on the Hough transform and phase portraits were developed to detect the ONH in fundus images of the retina.
- ❖ A success rate of 100% was achieved for the 40 DRIVE images using phase portrait analysis.
- ❖ Phase portrait analysis performed better than recently published methods with images from the DRIVE database.

Modeling and Parametric Representation of the Retinal Temporal Arcade

Faraz Oloumi, Rangaraj M. Rangayyan, Anna L. Ells

Department of Electrical and Computer Engineering
Schulich School of Engineering, University of Calgary
Division of Ophthalmology, Alberta Children's Hospital
Calgary, Alberta, Canada



SCHULICH
School of Engineering

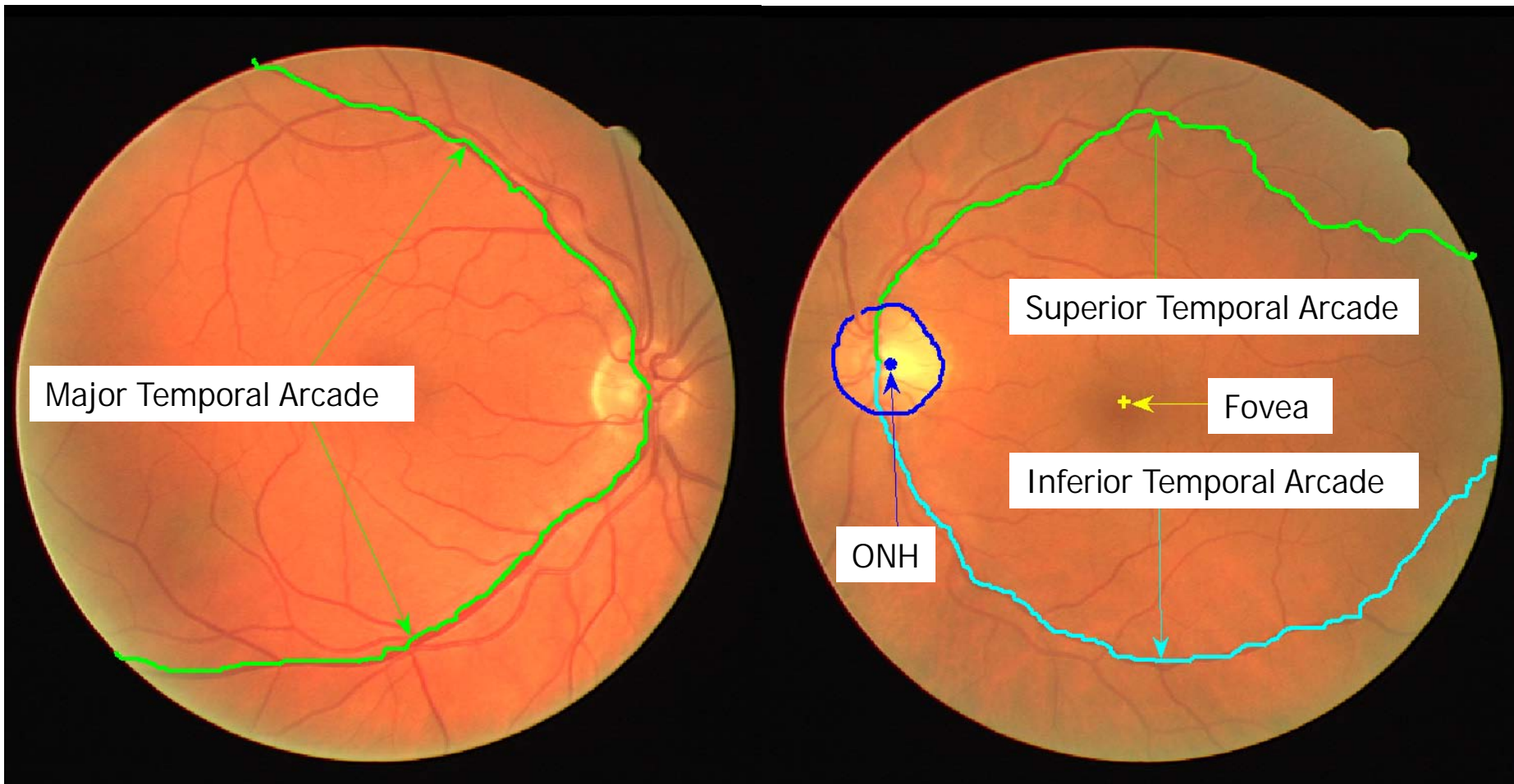


DEPARTMENT OF ELECTRICAL
AND COMPUTER ENGINEERING



UNIVERSITY OF
CALGARY

Retinal Temporal Arcade in Fundus Images





Retinopathy of Prematurity (ROP)

- ❖ The vessels in the retina are modified in terms of their width, shape, and tortuosity.
- ❖ ROP is the leading cause of preventable childhood blindness.
- ❖ Plus disease is used as an indicator of the severity of ROP.



Plus Disease

- ❖ Plus disease has been difficult to define in a quantitative manner.
- ❖ Diagnosis is made by visual, qualitative comparison.
- ❖ Abnormal dilation, tortuosity, and a decrease in the angle of insertion of the major temporal arcade (MTA) are symptoms of plus disease.



UNIVERSITY OF
CALGARY

Gold-standard Images



Two gold-standard images used as references for the diagnosis of dilation and tortuosity due to plus disease.



Limitations of Visual Comparative Analysis

- ❖ In a study to measure the level of agreement between experts there was:
 - 27% disagreement (18 of 67) on the presence of plus disease.
 - 37% and 31% disagreement on the presence of tortuosity and dilation due to plus disease.
- ❖ Computer algorithms needed for automated detection and analysis of retinal vessels.



Changes in Vessel Thickness and Tortuosity

- ❖ Venule thickness changes (of the order of 8 μm) are at, or below, the spatial resolution (20 $\mu\text{m}/\text{pixel}$) of retinal images.
- ❖ Arteriole tortuosity shows higher correlation to the presence of plus disease.
- ❖ Detection of arterioles presents an image processing challenge: arterioles are thinner than venules and have a lower contrast.



Angle of Insertion of the MTA

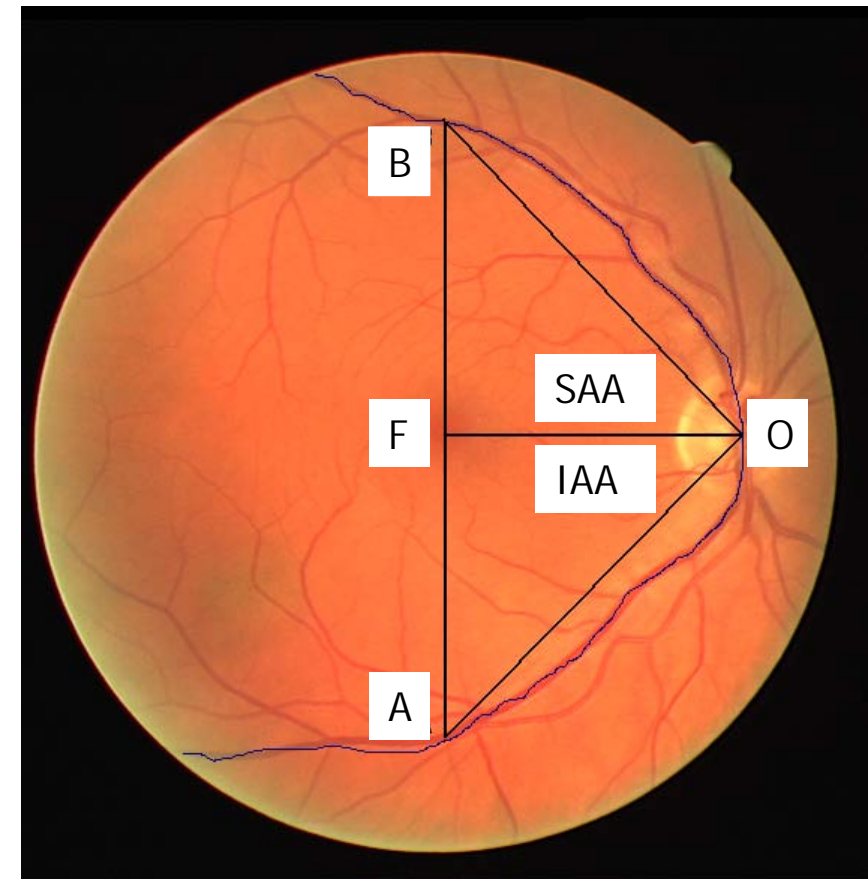
- ❖ There are inherent limitations in using vessel thickness and tortuosity as indicators.
- ❖ The angle of insertion of the MTA is an indicator of posterior structural integrity.
- ❖ A decrease in this angle can be a sequela of ROP.
- ❖ The temporal arcade angle (TAA) is defined by Wilson et al. as:

TAA = superior arcade angle (SAA) +
inferior arcade angle (IAA).



Angle of Insertion of the MTA

- ❖ Fovea (F) and ONH (O) are manually marked.
- ❖ The image is rotated so that the line OF (retinal raphe) is horizontal.
- ❖ The normal (AB) to OF is drawn at F up to the MTA.
- ❖ TAA = IAA + SAA
 - $SAA = \tan^{-1}(FB/OF)$
 - $IAA = \tan^{-1}(FA/OF)$.





Changes in the Angle of Insertion

- ❖ There is a high degree of symmetry between the angle of insertion of the two eyes of an individual.
- ❖ Asymmetry above 14° to 20° is suspicious.
- ❖ A significant level of vessel angle acuteness is associated between stages 0 and 1, stages 1 and 2, and stages 1 and 3 of ROP in the IAA of the left eye.



Detection of the MTA

- ❖ The MTA has not been modeled for quantitative analysis of its openness.
- ❖ The parabolic profile of the MTA could allow for effective modeling using the generalized Hough transform (GHT).
- ❖ Changes in the TAA are expected to be reflected as changes in the openness parameter of a parabolic model.



Parametric Modeling of the MTA

- ❖ Two steps in modeling the MTA:
 1. Derivation of a vessel map: magnitude output of the Gabor filter bank.
 2. Detection of parabolas: the generalized Hough transform.



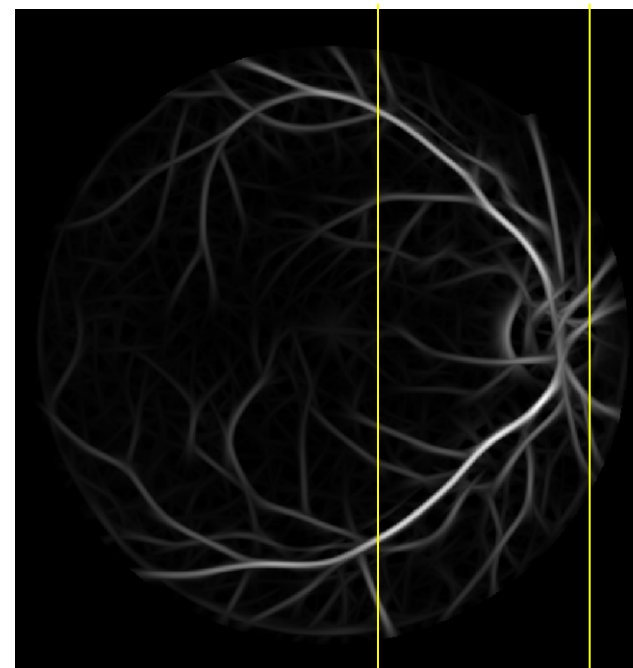
Derivation of the Vessel Map

- ❖ The magnitude output of the Gabor filters can be used for this purpose.
- ❖ A large value for thickness ($\tau = 16$) is used to emphasize the MTA with $I = 2$.
- ❖ The Gabor magnitude image is binarized using a fixed threshold.
- ❖ The binary image is skeletonized.
- ❖ The skeleton image is cleaned using the morphological area open procedure.

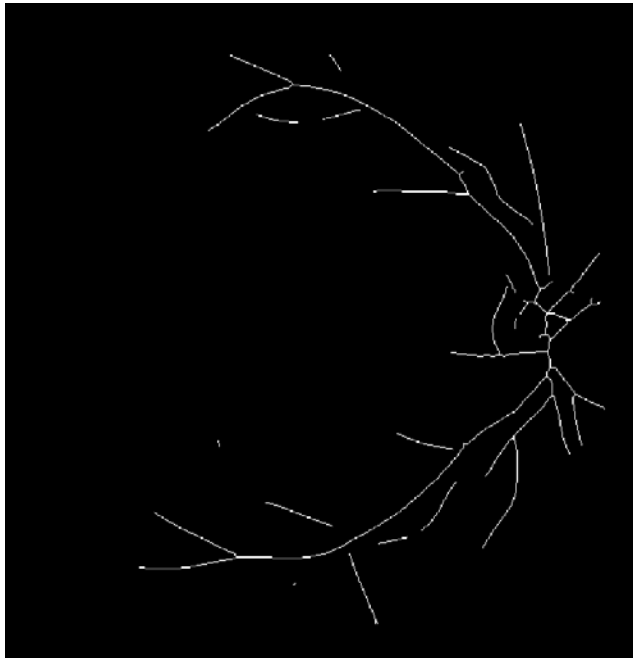
Original



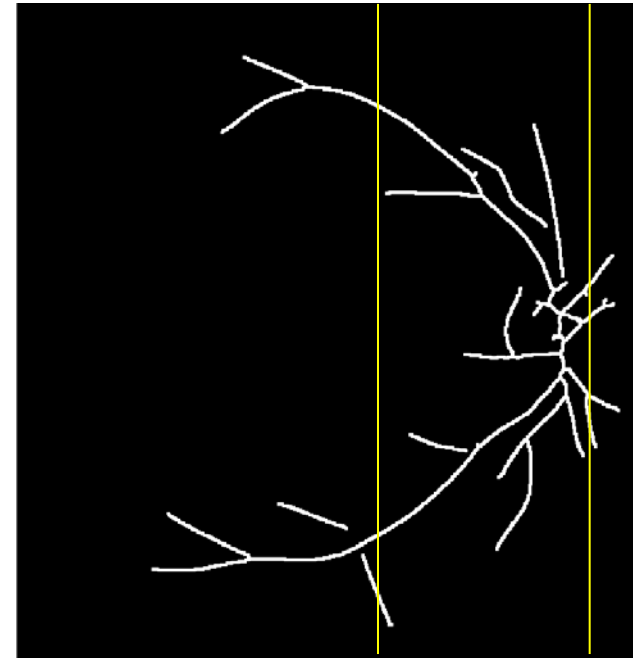
Vessel
Map



Skeleton



Cleaned
Skeleton





The GHT for Parabolic Modeling

- ❖ The GHT is a flexible method for parameterizing curves such as parabolas.
- ❖ The general formula defining a parabola:

$$(y - y_o)^2 = 4a(x - x_o)$$

where (x_o, y_o) is the vertex,
and a is the openness parameter.

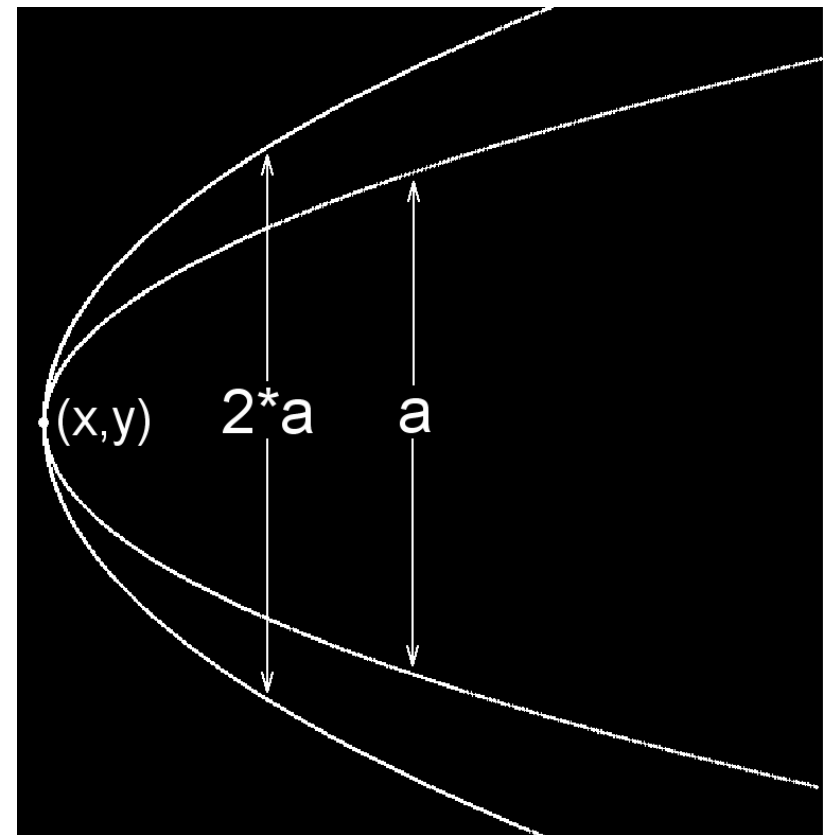


A Parabolic Model

The value of a defines the openness or aperture of the parabola and the direction it opens to; for a positive a value the parabola opens to the right and vice versa.

In this 584×565 image,

$$a = +59.$$





The GHT for Parabolic Modeling

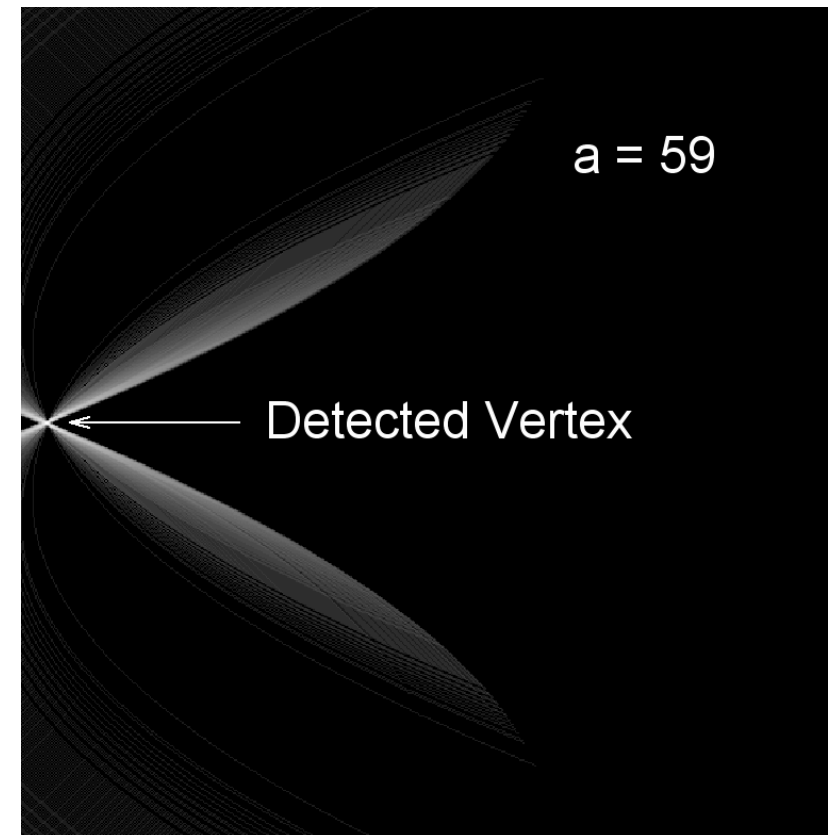
- ❖ The parameters (x_o, y_o, a) define the Hough space, represented by an accumulator A .
- ❖ For every non-zero pixel in the image domain, there exists a parabola in the Hough space for each value of a .
- ❖ A single point in the Hough space defines a parabola in the image domain.



Detection of the Parabolas

For every non-zero pixel in the image the parameter a is computed for each (x_o, y_o) in the Hough space and the accumulator is incremented.

The point with the highest value represents the best fitting parabola.



Hough space



Anatomical Restrictions on the Hough Space

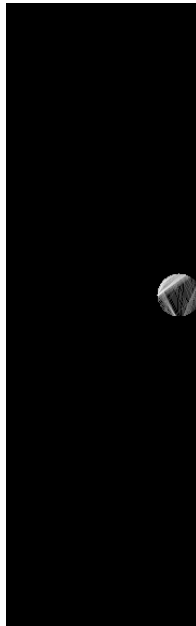
- ❖ The MTA follows a parabolic path up to the macula.
- ❖ Given that the macula is about 2 ONH diameters (ONHD) temporal to the ONH and prior knowledge of the ONH, we can restrict the horizontal size of the Hough space.
- ❖ Size of each plane is 584 x 170 pixels.



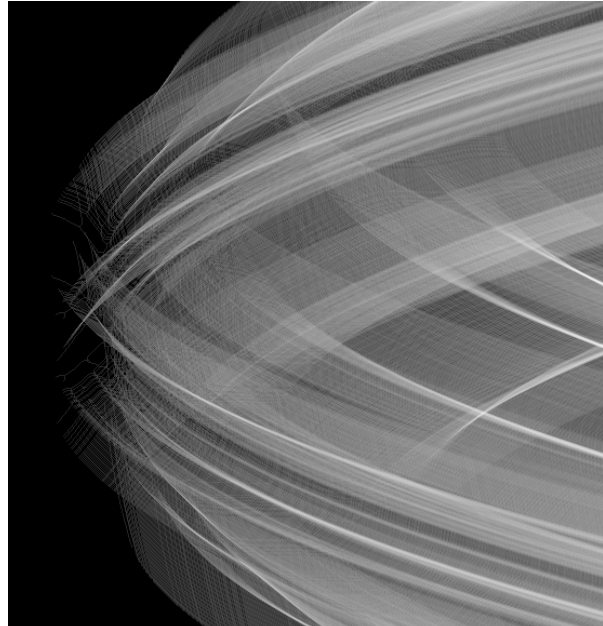
Anatomical Restrictions on the Hough Space

- ❖ The location of the vertex of the desired parabola in the Hough space is restricted to be within $0.25 * \text{ONHD}$ of the ONH.
- ❖ The value of a has a physiological limit: set to be within the range [35, 120] for DRIVE images.
- ❖ The number of planes in the 3D Hough space is 86.

Hough space updated with Gabor Mag. with vertex and horizontal size restrictions.



Hough space updated with unity with vertex and horizontal size restrictions.



Hough space updated with Gabor Mag. with horizontal size restriction.

Hough space updated with unity.



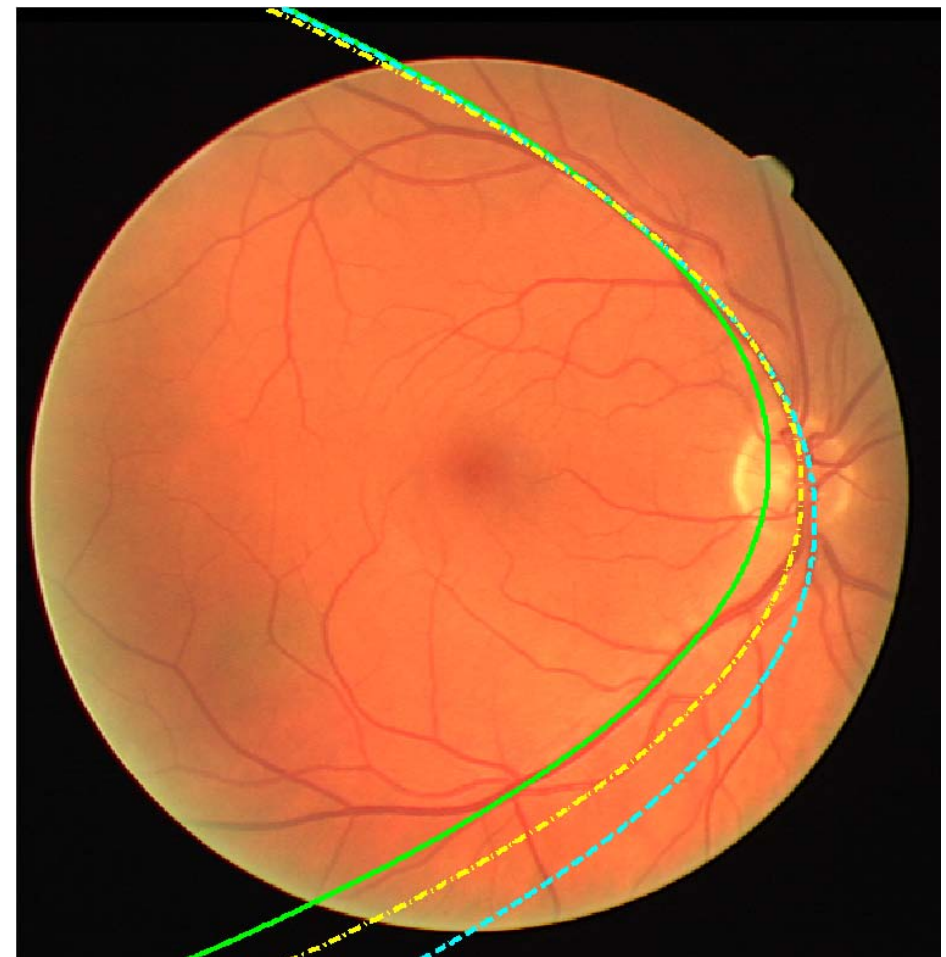
Parabolic Fits to the MTA

Global max. in the Hough space:

Gabor-magnitude-updated:
 $a = -65$

Gabor-magnitude-updated
with vertex restriction:
 $a = -75.$

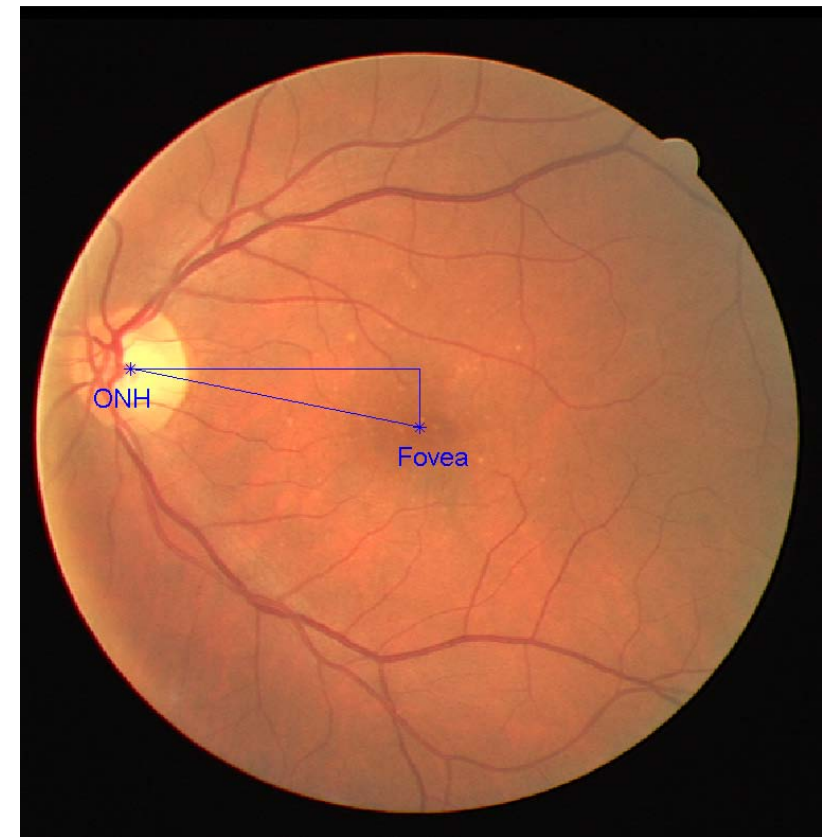
Unity-updated with vertex
restriction: $a = -66.$





Correction of the Retinal Raphe Angle

- ❖ The line going through the fovea and the center of the ONH is the retinal raphe.
- ❖ Any rotation that might exist between the retinal raphe and the horizontal axis of the image should be corrected.





Correction of the Retinal Raphe Angle

- ❖ The rotation angle was found automatically by using the manual markings of the ONH and the fovea.
- ❖ The original image was rotated by the determined angle by using bilinear interpolation and cropping the image to its original size.





MDCP Measure

- ❖ The MDCP measures the closeness of two given contours based on the mean of the distance to the closest point (DCP) from one of the contours (the model) to the other (the reference).
- ❖ Given a model, $M = \{m_1, m_2, \dots, m_N\}$, and a reference $R = \{r_1, r_2, \dots, r_K\}$, the DCP for a single point on M is defined as:

$$\text{DCP}(m_i, R) = \min \left(\|m_i - r_j\| \right), j = 1, 2, \dots, K$$

where $\| \cdot \|$ is a norm operator.



MDCP Measure

- ❖ The MDCP is computed as

$$\text{MDCP}(M, R) = \frac{1}{N} \sum_{i=1}^N \text{DCP}(m_i, R)$$

- ❖ The top 10 Hough-space candidates were selected for MDCP analysis.



Choosing Between the Top Hough-space Candidates

- ❖ By taking the parabolic fits to be the model (M) and the automatically obtained skeleton to be the reference (R), the MDCP was calculated for each of the top 10 candidates.

- ❖ The parabola with the lowest MDCP value was selected as the best fit to the MTA.



Dual-parabolic Modeling

- ❖ The ITA and the STA are often asymmetric; a single parabolic model may match either one of the arcades, but not both.
- ❖ Modeling each part of the arcade separately may be a more suitable option.
- ❖ To represent the ITA, any information above the detected center of the ONH was eliminated in the Gabor magnitude response image.



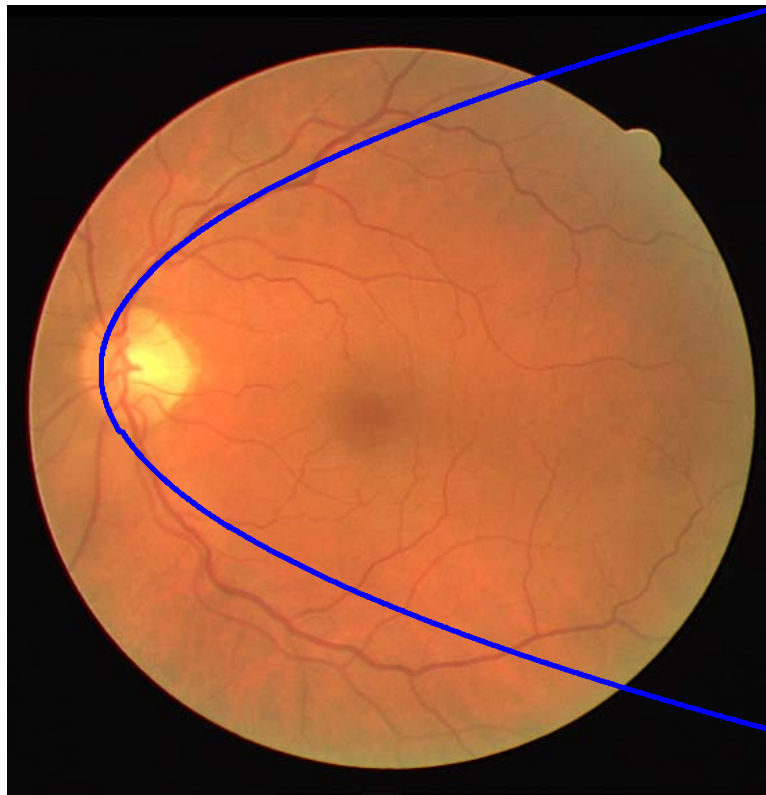
Dual-parabolic Modeling

- ❖ The STA was represented by excluding the information in the Gabor magnitude response image below the detected center of the ONH.
- ❖ The upper part of the parabolic fit to the STA was taken as the STA model.
- ❖ The lower part of the parabolic fit to the ITA was taken as the ITA model.

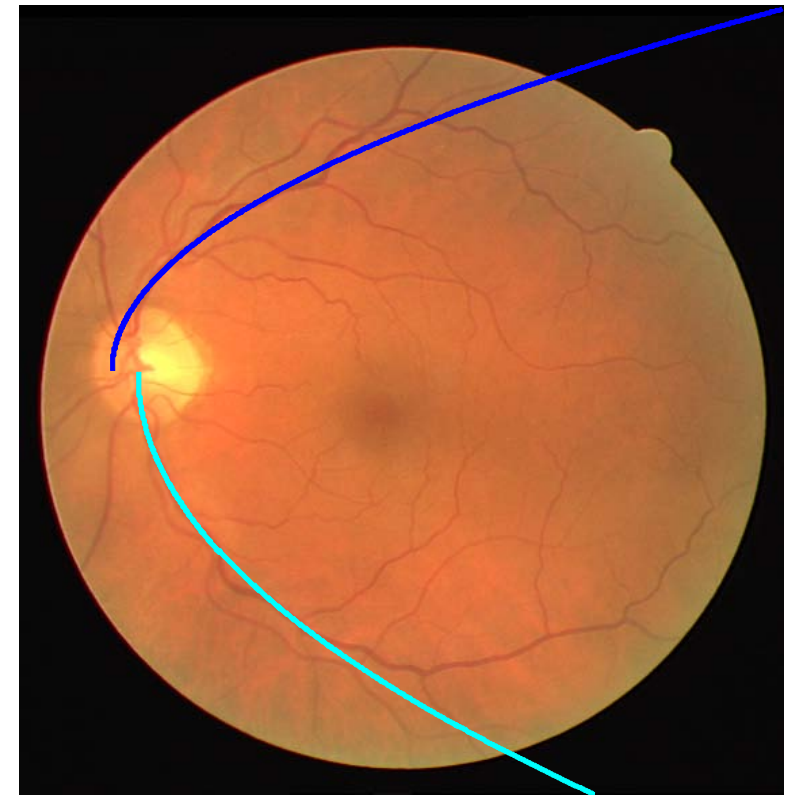


UNIVERSITY OF
CALGARY

Dual-parabolic Modeling



Parabolic fit using Gabor-magnitude-updated GHT



Dual-parabolic fit using
Gabor-magnitude-updated GHT ¹⁰⁸



Performance Measures

- ❖ The MTAs for all 40 DRIVE images were drawn by an expert ophthalmologist.
- ❖ Two types of performance measure:
 1. The accuracy of the parabolic model fitted to the vessel skeleton (Auto) as compared to the parabolic model fitted to the hand-drawn contour (Hand).
 2. The accuracy of the parabolic model fitted to the vessel skeleton as compared to the hand-drawn contour.

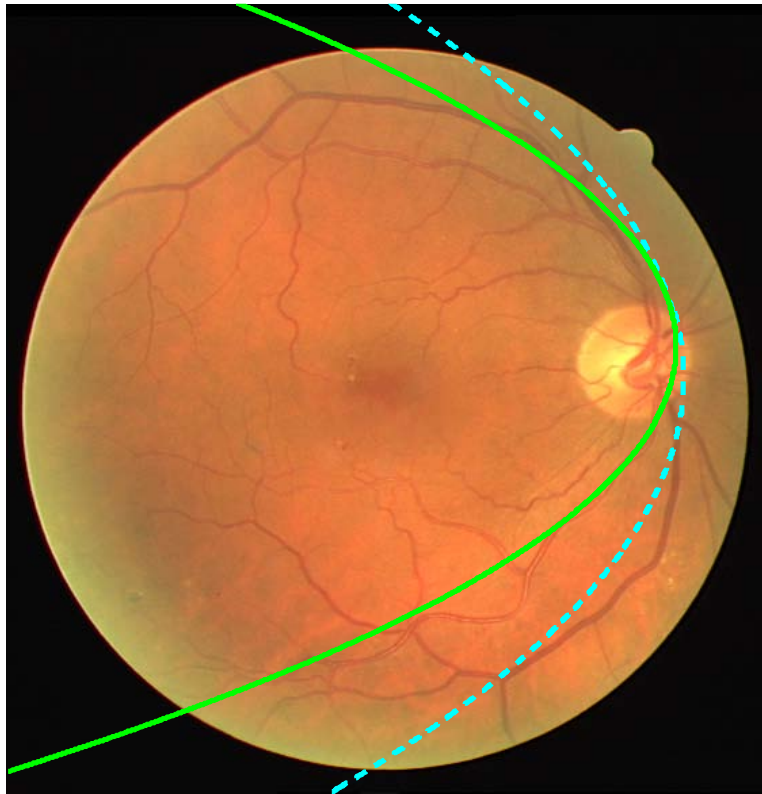


Comparing the Parabolic Models

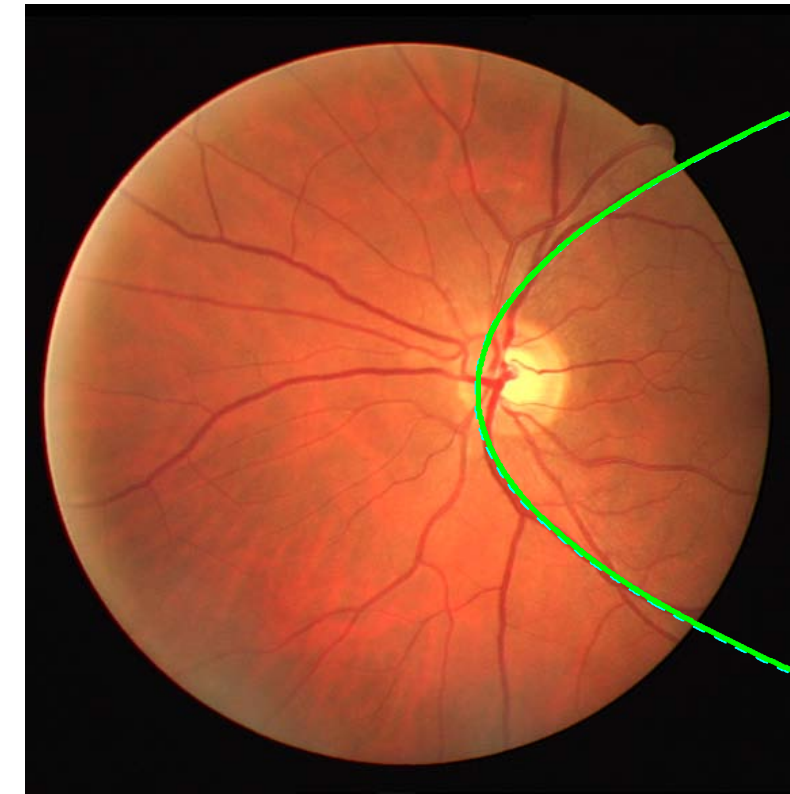
- ❖ The fits to the hand-drawn traces were obtained using all versions of the Hough space.
 - ❖ A distance error measure was obtained in terms of the Euclidean distance between the two detected vertices as:
- $$\sqrt{(x_{o_{Hand}} - x_{o_{Auto}})^2 + (y_{o_{Hand}} - y_{o_{Auto}})^2}$$
- ❖ The correlation coefficient between the two sets of a values was also computed:
$$\frac{C(a_{Hand}, a_{Auto})}{\sqrt{C(a_{Auto}, a_{Auto})C(a_{Hand}, a_{Hand})}}$$
where C is the covariance.



Results of Parabolic Modeling



The automatic fit (solid green)
is matching the arteriole.



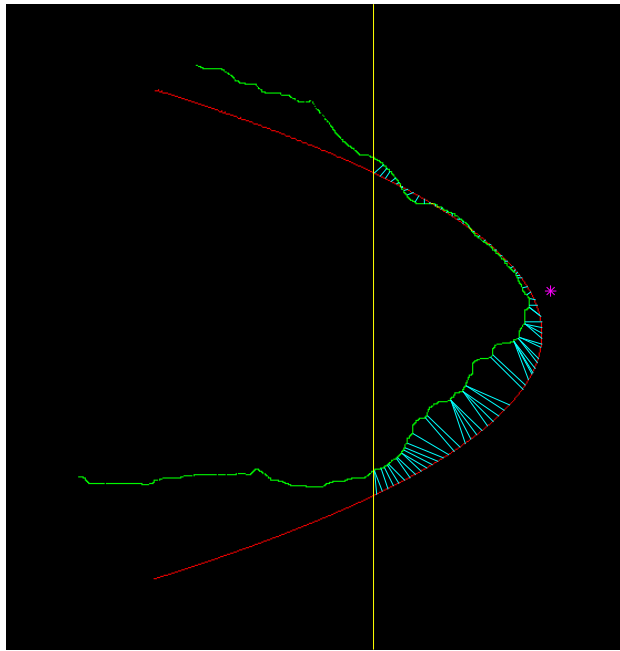
Both fits are accurate.
Cyan: fit to hand-drawn MTA. **111**



Accuracy of the Parabolic Model

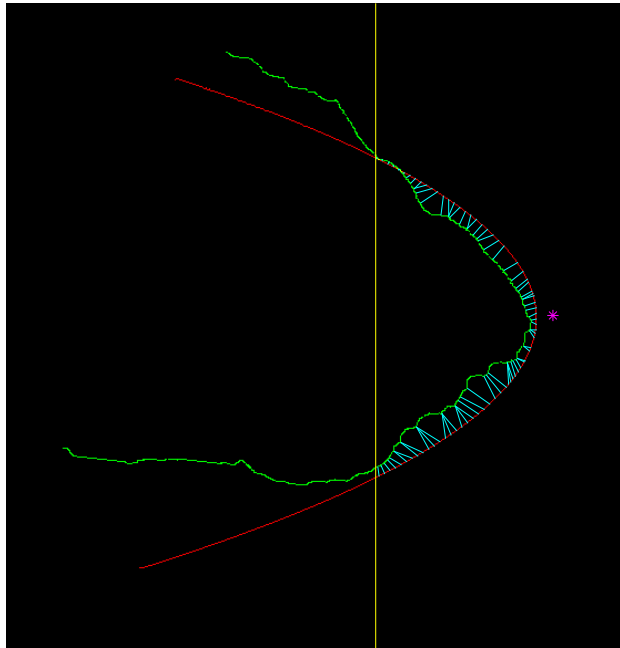
- ❖ To assess the accuracy of the obtained parabolic fits compared to the hand-drawn MTA, the MDCP was used as a distance error measure.
- ❖ Parabolic fits were obtained using the four versions of GHT as described before with the added options of MDCP-based selection and correction of the raphe angle.

MDCP =
17.63
pixels



With
vertex
restriction
MDCP =
25.04
pixels

With
raphe
angle
correction
MDCP =
12.63
pixels

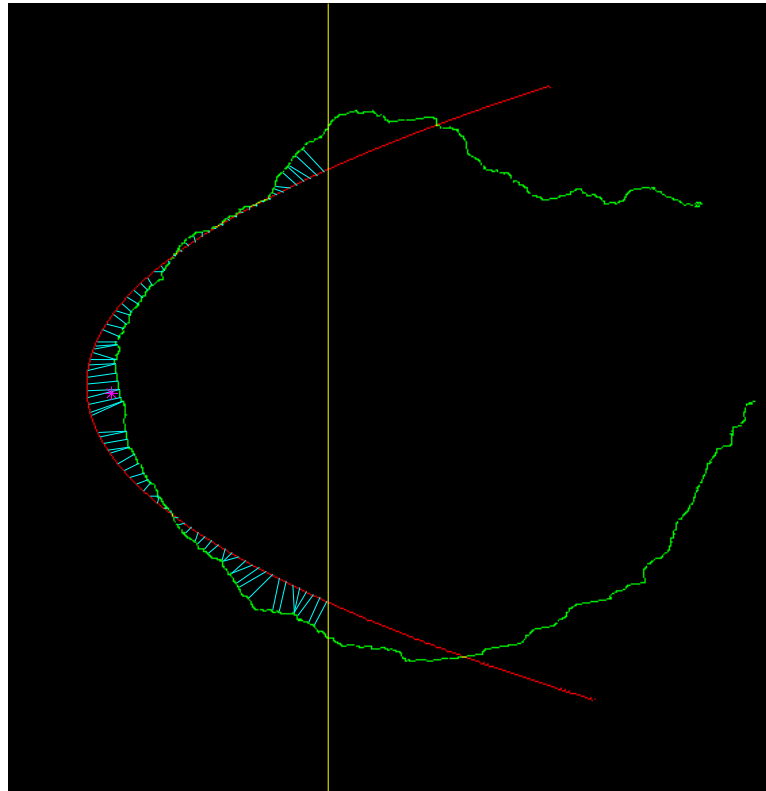


With
MDCP-
based
selection
MDCP =
12.33
pixels.

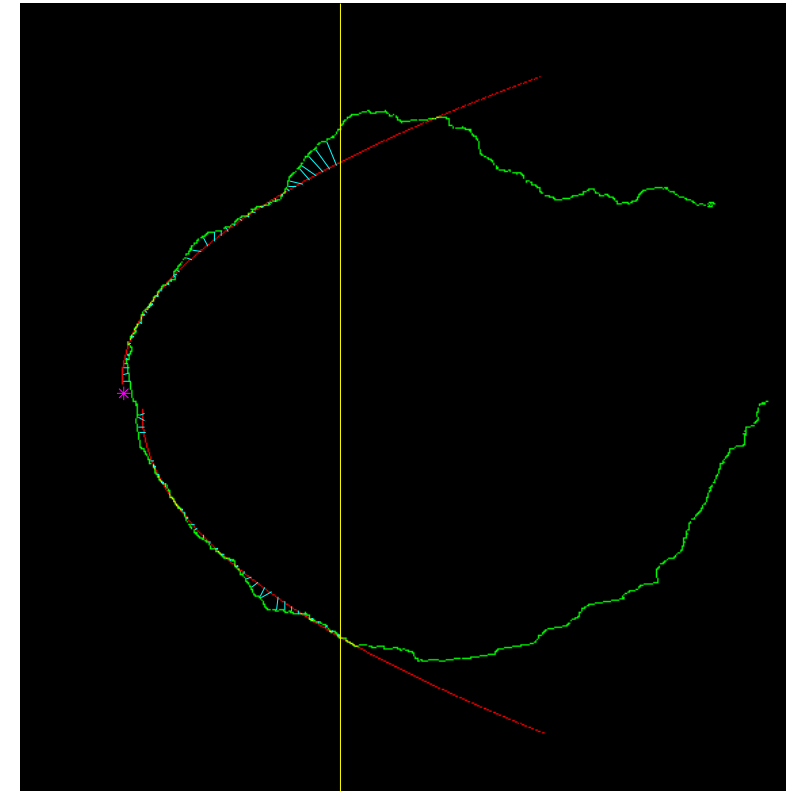


UNIVERSITY OF
CALGARY

Results: Dual-parabolic Modeling



Single model: MDCP = 11.5



Dual model: MDCP = 3.11

GHT Version	MDCP, Mean \pm STD [pixels]	With raphe- angle correction	With MDCP- based selection	With raphe- angle correction And MDCP- based selection
Unity-updated	18.35 \pm 11.40	16.62 \pm 9.42	16.26 \pm 9.93	14.20 \pm 7.07
Unity-updated with vertex restriction	16.27 \pm 8.84	15.09 \pm 7.85	15.15 \pm 8.13	13.45 \pm 7.54
Gabor-magnitude-updated	14.08 \pm 9.93	13.93 \pm 9.20	12.68 \pm 8.80	12.79 \pm 8.63
Gabor-magnitude-updated with vertex restriction	16.06 \pm 9.05	12.64 \pm 6.39	14.59 \pm 8.00	12.10 \pm 6.16
ITA Model	12.07 \pm 8.88	12.33 \pm 11.02	10.90 \pm 8.71	10.64 \pm 8.76
STA Model	15.01 \pm 16.32	14.09 \pm 15.28	14.52 \pm 16.71	13.93 \pm 16.06



Remarks

- ❖ Parabolic modeling could assist in quantitative analysis of changes in retinal vasculature.
- ❖ Two factors causing inaccuracy in the models:
 1. Distinct presence of arterioles and other vessels: a procedure to detect and eliminate arterioles may be used.
 2. High slope of arcades at the ONH: An exponential model fitted to each arcade separately may lead to better models.



UNIVERSITY OF
CALGARY

Graphical User Interface

AnalysisOfRetinalVasculature

File Help View

Select an Image to Process

Look in: test

Recent Places

Desktop

Libraries

Computer

Network

diaretdb1 image... diaretdb1 image... diaretdb1 image... diaretdb1 image...

diaretdb1 image... diaretdb1 image01 2.png

File name: diaretdb1_image012.png

Open

Cancel

Files of type: (*.jpg, *.jpeg, *.jpe, *.jfif, *.tiff, *.tif, *.bmp, *.gif, *)



Detection of Blood Vessels

Gabor Filter Parameters

Tau: [] Blood vessel thickness (Default Tau = 16 pixels)

L: [] Blood vessel elongation (Default L = 2)

K: [] Number of filters (Default K = 45)

Gabor Filter Input Image

Y Component Green Component

Run Gabor Filters

Binarization of the Detected Vessels

Threshold: []

How many connected pixels to remove: [] 0 Remove

Modeling of the Temporal Arcade

This is an image of the: OD (Right Eye) OS (Left Eye)

Single-Parabolic Modeling (MTA) Save ...

Dual-Parabolic Modeling (ITA & STA)

Measurement of the Arcade Angle

Method of Wilson et al. Method of Wong et al.

Image to Use for Marking: Green Channel Color

Image Scale Factor: x 1 x 1.5 x 2

Radius of Circle Save ... Start

7:13 PM 19/07/2012



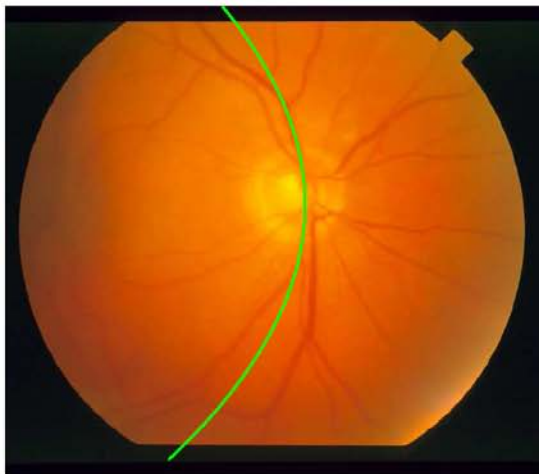
Method of Wong et al.

- ❖ Mark the center of the ONH.
- ❖ Center image on the ONH.
- ❖ Crop image to circle of diameter 240 pixels.
- ❖ Manually mark the largest venule branches.
- ❖ Vertex of the angle is the center of the ONH.
- ❖ Two points marked at the intersection of a circle of radius 60 pixels with the venule branch to define the arcade angle.

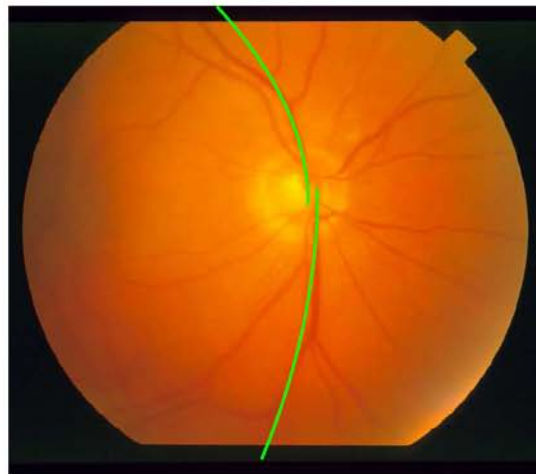


UNIVERSITY OF
CALGARY

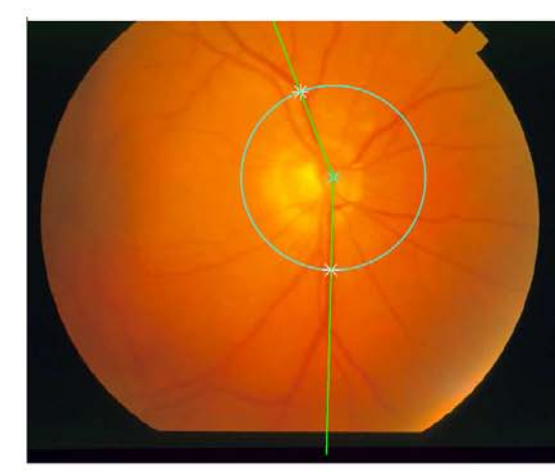
Results: Application to PDR



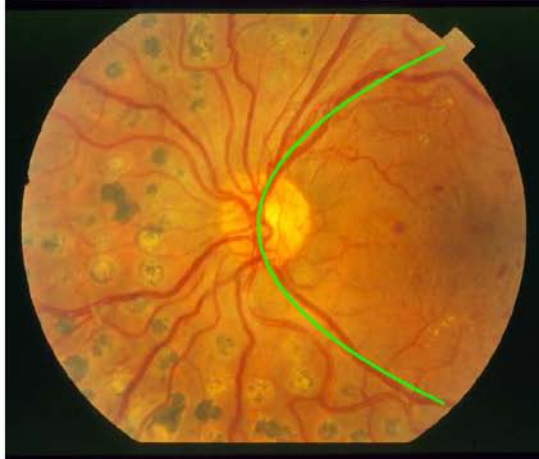
Normal: $aMTA = -153$



$aSTA = -138$, $aITA = -420$



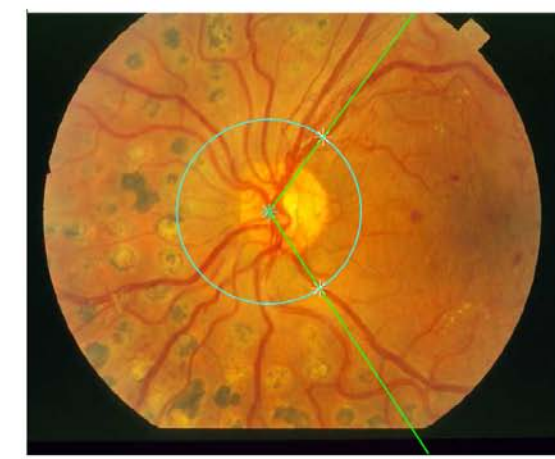
$TAA = 157.8^\circ$



PDA: $aMTA = 55$



$aSTA = 36$, $aITA = 48$



$TAA = 110.4^\circ$



PDR: ROC Analysis

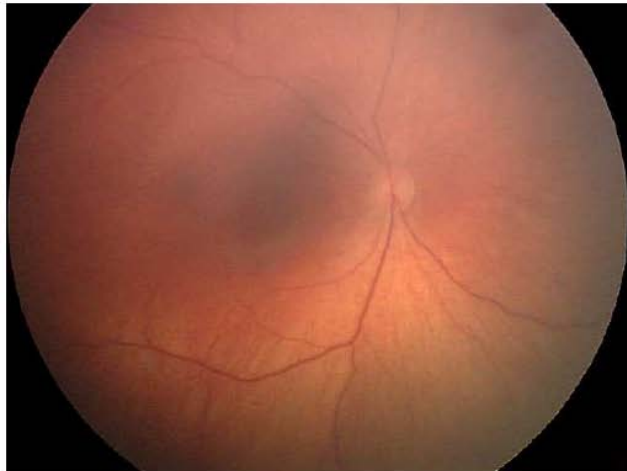
Parameter	Normal	PDR		A_z (SE)	<i>p</i> -value
	(<i>n</i> = 11)	(<i>n</i> = 11)	Mean \pm STD		
Arcade Angle (Degrees)	151.00 ± 11.23	139.01 ± 11.96		0.80 (0.093)	0.0156
$ a_{MTA} $	140.40 ± 61.35	86.27 ± 26.76		0.87 (0.096)	0.0026
$ a_{STA} $	84.93 ± 27.66	88.36 ± 46.28		0.49 (0.122)	0.7839
$ a_{ITA} $	166.80 ± 98.72	89.18 ± 51.43		0.82 (0.088)	0.0164



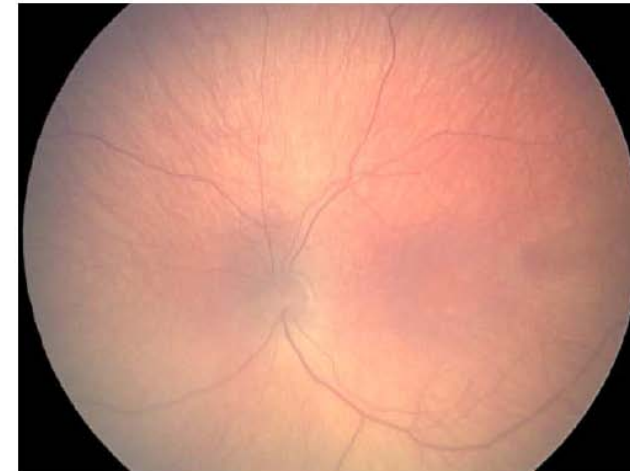
UNIVERSITY OF
CALGARY

Results: Application to RoP

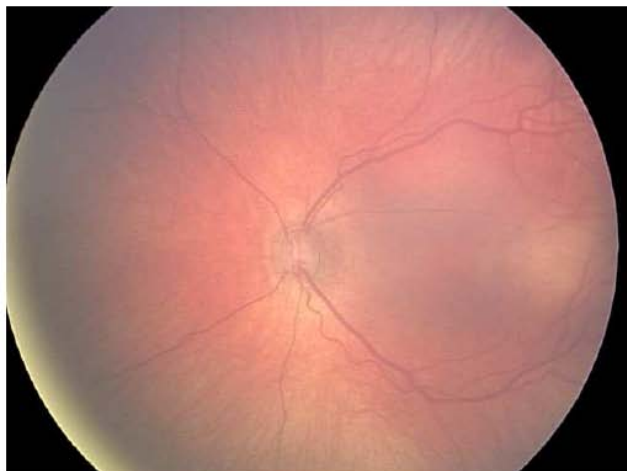
RoP 0



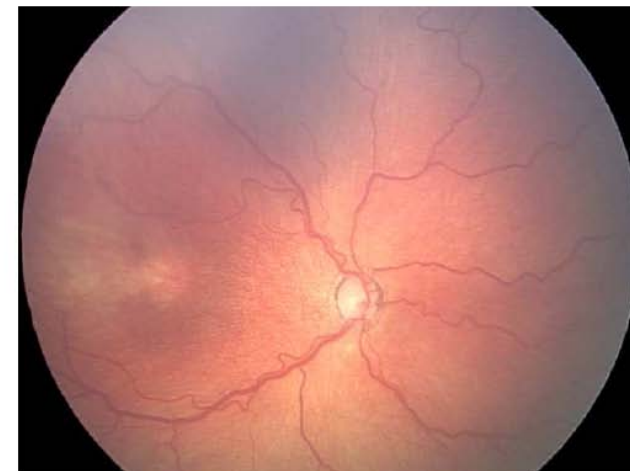
RoP 1



RoP 2



RoP 3





Results: Application to RoP

Parameter	Stage 0, Mean \pm STD	Stage 1, Mean \pm STD	Stage 2, Mean \pm STD	Stage 3, Mean \pm STD
Arcade Angle	119.98 ± 15.79	116.92 ± 18.35	107.58 ± 12.18	106.20 ± 15.63
$ a_{MTA} $	54.28 ± 33.53	39.06 ± 14.75	35.72 ± 20.27	36.00 ± 39.74
$ a_{STA} $	56.11 ± 47.11	56.00 ± 81.62	37.17 ± 17.70	34.22 ± 24.34
$ a_{ITA} $	69.83 ± 67.32	70.89 ± 83.13	40.50 ± 21.91	44.83 ± 59.01



RoP: ROC Analysis

ROP Stage	Arcade Angle, A_z (SE)	$ a_{MTA} $, A_z (SE)	$ a_{STA} $, A_z (SE)	$ a_{ITA} $, A_z (SE)
0 vs. 1	0.55 (0.095)	0.67 (0.088)	0.57 (0.095)	0.50 (0.095)
0 vs. 2	0.73 (0.083)	0.71 (0.085)	0.62 (0.093)	0.67 (0.088)
0 vs. 3	0.74 (0.081)	0.75 (0.083)	0.69 (0.087)	0.75 (0.081)
0 vs. 2 + 3	0.74 (0.069)	0.73 (0.068)	0.66 (0.079)	0.71 (0.072)
0 vs. 1 + 2 + 3	0.64 (0.068)	0.71 (0.067)	0.64 (0.078)	0.65 (0.072)



Remarks

- ❖ The method of Wilson et al. is inapplicable to most cases of PDR used in this work.
- ❖ The radius of the circle in the method of Wong et al. affects the arcade angle.
- ❖ No other study has quantitatively measured the narrowing of the MTA due to PDR.
- ❖ The parameters of the parabolic model could assist in diagnosis and follow up.



UNIVERSITY OF
CALGARY

Thank You!

Natural Sciences and Engineering
Research Council of Canada.

My students, coworkers, and collaborators.